APPLICATIONS OF LAMBDA RHO AND MU RHO INVERSION FOR CHARACTERIZATION OF LOWER GORU C SANDS

By

Fahad Ali Sajid

ID No:02112013014

A thesis submitted to Quaid-e-Azam University, Islamabad in partial fulfillment of the requirement for the degree of M phill in Geophysics

Department of Earth science

Quaid-i-Azam University

Islamabad Pakistan

2022

APPLICATIONS OF LAMBDA RHO AND MU RHO INVERSION FOR CHARACTERIZATION OF LOWER GORU C SANDS

By

Fahad Ali Sajid

ID No:02112013014

Department of Earth science

Quaid-i-Azam University

Islamabad Pakistan

2022

ACKNOWLEDGEMENT

In the name of Allah, the most Beneficent and the most Merciful, on whom ultimately, we depend for sustenance and guidance. I bear witness that Holy Prophet Muhammad (PBUH) is the last messenger, whose life is perfect model for the whole main kind till the day of the judgment. First, I gratitude to Allah Almighty whom blessing always upon me in my whole life. Without Him I am nothing. He has given me strength and capable me to complete my thesis. I am especially grateful to my honorable supervisor Dr. Amir Ali whom guidance and appreciation during thesis work enable us to learn more from him. He gave me his precious time during whole study work. I am also thankful to my seniors Yawar Amin, Ferhana Masood, their guidance cooperation, and help during whole thesis work. I am also thankful to my brother Saad Ali Sajid and friends Abdul Majeed, Usama and my other class fellows, their support during this work enable my work easier to me. I specially acknowledge the prayers and efforts of my whole family, especially my parents and my siblings for their encouragement their support and sacrifices throughout the study. I also wish to thank the whole faculty of my department for providing me with an academic base which has enabled me to complete my thesis work. I am also thankful to the employees of clerical office who helped me a lot and all those their names do not appear here who have contributed to the successful completion of this study.

Dedication To my Beloved Family

ABSTRACT

The exploration and exploitation of hydrocarbons as the main source of energy is vital for the economy of any country. Every sedimentary reservoir requires a detailed analysis prior to extraction for optimal production. The main objective of this research is to find and spatially characterize the prospect zones in the sands of Lower Goru Formation in Gambat area, geographically located about 42 km south-west of the producing Sawan Gas field. The study for the structural interpretation and reservoir analysis of Gambat area has been conducted using 3D seismic data and well log analysis. Horizons have been marked along the formation tops based upon the seismic-to-well-tie. Time and depth contours maps have been generated for the formations of interest to analyze their spatial extension and regional structures. Model-based inversion has been applied to the 3D seismic data for estimation of acoustic impedance values. A regression line-based equation has been developed for the cross-plot of effective porosity and impedance values to spatially mark the distribution of effective porosity. Furthermore, the Lambda-Rho ($\lambda\rho$) and Mu-Rho ($\mu\rho$) sections and their respective slices have been developed to analyze to fluid content and lithology within the zone of interest of the C interval. The seismic interpretation shows the presence of normal faults indicating the extensional regime. The petrophysical analysis indicates a zone of interest in the C sand interval of the Lower Goru Formation with shale volume of 39.4%, and effective porosity of 12.6%, and water saturation of 12.6% and hydrocarbon saturation is 87.4% This zone is spatially indicated by the low impedance values within the C interval from the results of the model-based inversion. Furthermore, the effective porosity distribution also indicates high porosities along the zone of interest throughout the interval. The borehole-derived porosity and the porosity values determined from post-stack inversion at the specified well locations are very close indicating the accuracy of the applied technique. The presence gas along the zone of interest is confirmed by the low $\lambda\rho$ values with the moderate values of $\mu\rho$ depicting the presence of sand lithology.

TABLE OF CONTENTS

CHAPTER 3
SEISMIC DATA INTERPRETATION

CHAPTER 4
PETROPHYSICS

LIST OF FIGURES

CHAPTER 1

INTRODUCTION

1.1 Study area

The study area selected for carrying out this research is the Gambat block, Khairpur District, Sindh, Pakistan as shown in figure 1.1. It is located in the Thar platform of the Southern Indus Basin. The first seismic acquisition survey carried out in this area in the year 1986.

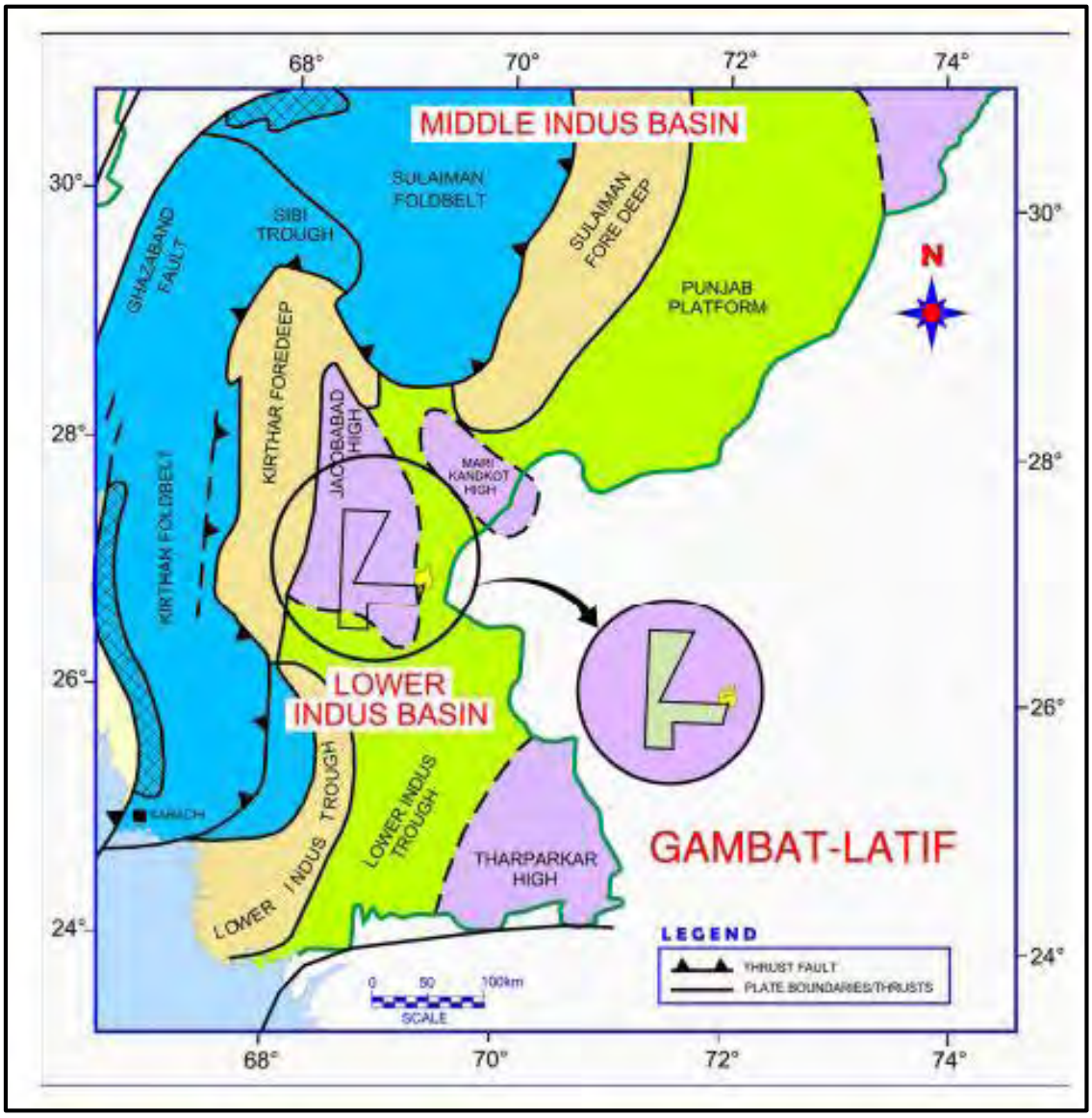

Figure 1.1: Tectonic map of Gambat Latif area (modified from Kazmi and Rana 1982).

1.2 Exploration History

From literature review, the exploratory history of the Tajjal gas field states that seismic survey was first carried out by OGDCL in 1986 and later by BRITISH GAS in 1996. In 2007, the first discovery of Tajj-01 was made by extended well testing which produced gas at rate of 25 million scf/d (4,000 BOE/d) which in turns discovered the Tajjal gas field. The gas produced is transported by 20km pipelines to Sawan Gas Processing plant. SNGPL, a gas buyer distributes it to Northern Pakistan. Official operator of the field is OMV 35% along its Joint ventures PPL30%, ENI30% and GHPL5% (Government holding Pakistan Limited).

1.3 Objectives of Research Work

Objectives of dissertation are as follows:

- To map the spatial extension of formation tops as horizons and identify the subsurface structures.
- To identify and evaluate the zone of interest within the sands of Lower Goru Formation based on petrophysical analysis.
- To confirm the spatial distribution of prospect zone using Model-based inversion.
- To generate the sections of lambda-Rho (λρ) and Mu-Rho (μρ) for confirming the presence of fluid and the lithology within the zone of interest
- To map the effective porosity distribution for the zone of interest in order to determine the extent of the prospect zone.

1.4 Data requirements

Following public domain 3D Seismic data cube of Gambat Latif Block will be acquired from DGPC along with three wells Tajjal-01, Tajjal-02 and Tajjal-03 on behalf of recommendation letter from E&ES Department Quaid e Azam University, to achieve the desired research objectives. Provided data includes the following data sets:

- 3D Seismic cube of Gambat Latif Block
- Navigation files
- Digital Well Data
- Formations Tops

1.4.1 Seismic lines

Migrated seismic sections and SEG-Y's of following seismic lines

1.4.2 Well data

Complete suite of logs is required for following wells for the intended research work:

- Tajjal-01
- Tajjal -02
- Tajjal-03

1.5 Base map

It's a kind of map that displays orientation and location of the seismic lines along with projected wells that can be used as reference is known as base map as shown in figure 1.1.

1.6 Methodology:

The methodology we used in this whole process of the research is given below

1) Literature Review
2) Generation of synthetic seismogram
3) Marking of horizons and faults
4) Time picking
5) Constructing TWT contour maps
6) Velocity analysis by multiple velocities
7) Construction of depth contour maps
8) Seismic inversion
9) Petro physical analysis by means of well log data

CHAPTER 2
GEOLOGY AND STRATIGRAPHY

2.1 Overview

The largest sedimentary basin in Pakistan is the Indus basin. There is an Indian craton to the east of the Indian basin, the Kohat Potwar plateau to the north, and the Suleiman and Kirthar ranges' fold and thrust belts to the west. NE-SW oriented basin has a length along its axis of around 1600 km and a width of 300 km. While some steeply dipping structural features are also present, exposing the basement rocks primarily as Sargodha Highs in the NE and Naggar Parker Highs in the SE, it primarily consists of normal to moderately dipping structural features. The separation of the Indus basin into the Upper and Lower Indus basins is the result of the tectonic plates' compression regime. Between the Lower and Upper Indus basins is Jacobabad High. The center and southern Indus basins make up the Lower Indus basin (Kadri, 1995). Within the Southern Indus basin is the study area. The current Indus basin was located at the continental side of the Indian plate, which is actually the southernmost landmass of Gondwana, from the Permian to the Middle Jurassic. During the Late Jurassic and Early Cretaceous, rifting began. Later, the Indian Plate moved north and clashed with the Eurasian Plate in the Tertiary (Kadri, 1995). Pakistan's territorial limits straddle the Indo-Pakistan, Arabian, and Eurasian plates, with their triple junctions situated to the north-west of Karachi. Pakistan is positioned along the tertiary convergence zone, which is where three lithospheric plates meet. There is a sizable sedimentary region there that offers potential for petroleum. A total of 828,800 km2 of onshore and offshore sedimentary area and 3,791,060 km2 of sedimentary volume were occupied by Pakistan. Gondwana maintained its identity until the Permian. Early in the Cretaceous, the Madagascar plate and the Indo-pak plate split apart. Indian plate moved northward from the late Jurassic to the early Cretaceous, and subsequently, in the Tertiary, it collided with Eurasian plate (Kazmi and Jan, 1997).

The research area is located on the eastern and southern shoulders of the Khairpur high, which is causing a regional north-south trend. This mountain played a crucial role in the development of hydrocarbon-bearing traps around it and inside the research region (Kazmi and

Jan, 1997). The area's three most important gas fields are Kadanwari, Sawan, and Miano, which have been producing gas from Lower Goru Formation sands. There are numerous other gas fields as well that are producing from Eocene carbonates (with low to medium combustibility with large inert gases) as well. The area is known for the presence of stratigraphic and structural traps (Kadri, 1995). The area is known to have been recognized by three post-rifting tectonic events; uplift and inversion in late cretaceous, right lateral strike slip faulting in late Paleocene and a late tertiary to Holocene uplift of the Khairpur high. Wells drilled in the Tajjal area have been observed by the high geothermal gradient up to4.8 dgc/100m (328ft), Pre Triassic-sediments have not drilled yet in this region. The platform carbonates and the lowermost clastic layers of the Cretaceous show an unconformity or an erosional phase of varying length. these Cretaceous clastic sediments. The Sembar Formation and Lower Goru Formation are clastic rocks found on the Indian Plate's western shelf (Kadri, 1995) (Figure 2.1)

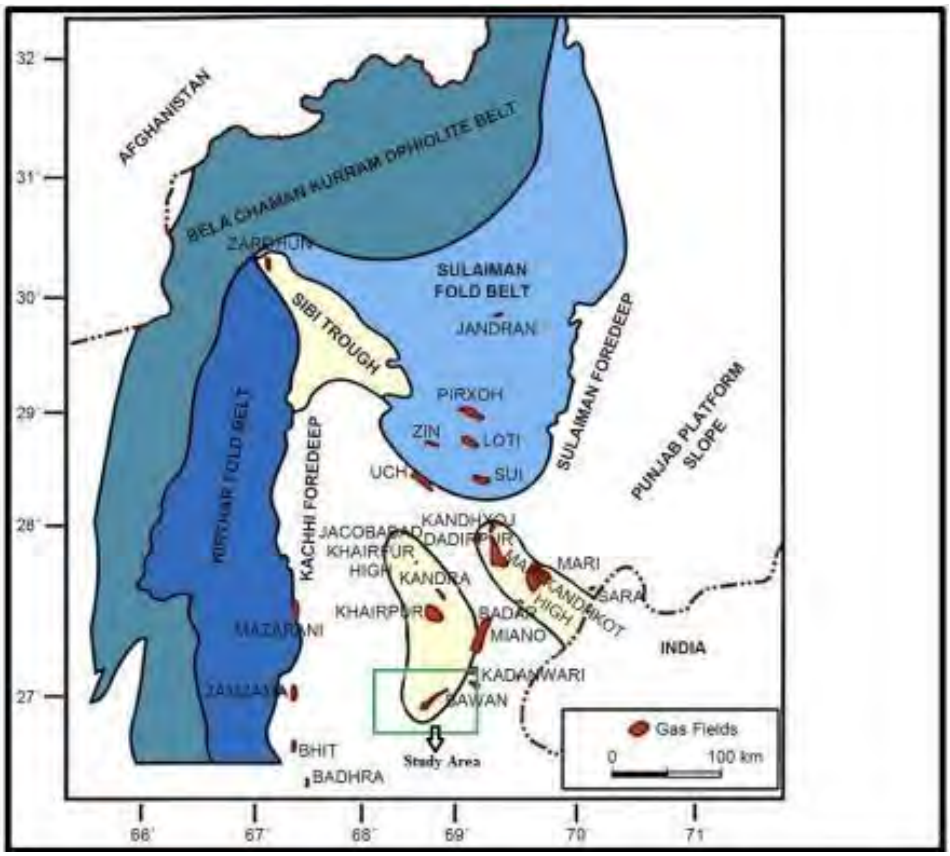

Figure 2.1: Geological map of Gambat Latif southern Indus Basin (Krios et al., 1998).

2.2 Structural style of Gambat Area

The platform is one of the Southern Indus Basin's four divisions. It has a monocline-like inclination that resembles a platform in Punjab. The Indian shield's surfaces are reflecting in Nagar Parkar High's terminology as the sedimentary wedge thins away. This is different from the Punjab platform because it exhibits the signature of extension tectonism as a result of the most recent counterclockwise movement of the Indian plate. As a result, the research area is under an extensional regime and there is normal faulting in the region. These circumstances lead to the formation of negative flower structures in the vicinity (Kadri, 1995). In the north of the study region are the Sulaiman fold belt and Sulaiman foredeep; to the east and west are the Kirthar fold belt and Karachi foredeep, respectively. Sindh Monocline and Karachi trough in South of Gambat (Kadri, 1995).

2.3 Generalized stratigraphy of the area

Stratigraphy of study area generally varies from Sembar Formation of early Cretaceous period to Siwaliks group of Miocene Pliocene Epochs of Quaternary periods. Sembar formation having Type 3 kerogen, TOC>15% and is Gas generation phase is proven source rock of the area. There is a unconformity or depositional gap of 30Ma between organic rich shales of Sembar of early Berriasian (145.6 Ma) to Lower Goru sands of Alibian (112 Ma) (Nazeer et al., 2012). Sembar Formation is prograding west margin the basin direction with younger ages and becomes older towards East. A interval and B Interval deposited in Lower Cretaceous, while C and D sands members of Lower Goru along with shale interval above them deposited in Upper Cretaceous period. Sui Main Limestone and Habib Rahi Limestone are other main reservoirs but not acting as reservoir in this area (Figure 2.2).

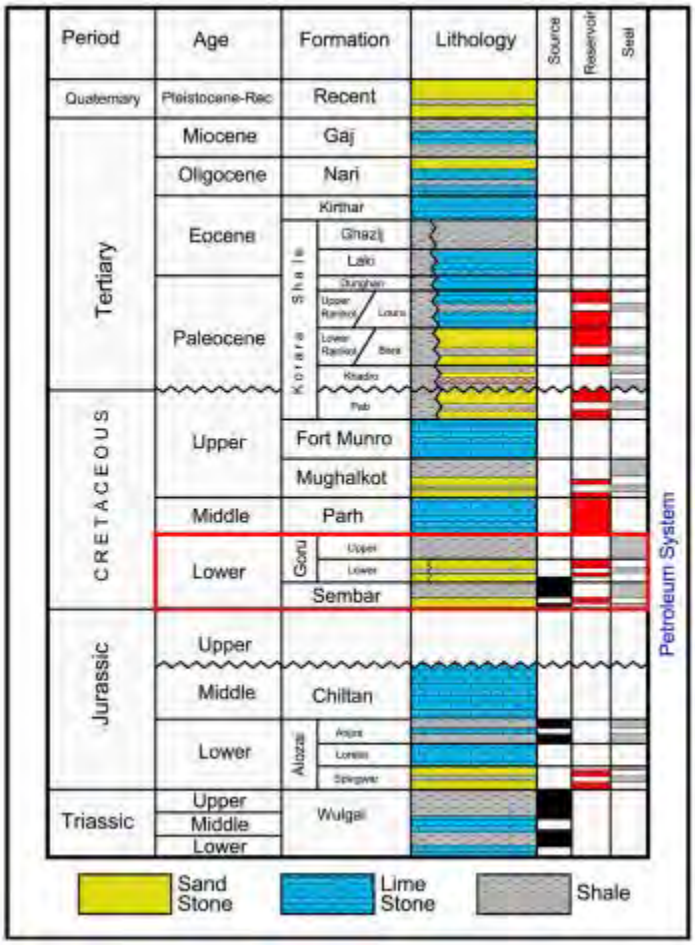

Figure 2.2 Stratigraphy of the Lower Indus Basin specifying our source reservoir and seal Abbasi et al. (2016).

2.4 Borehole stratigraphy

2.4.1 Sembar Formation

A known source rock in the region is the Sembar Formation, which is late Jurassic to Early Cretaceous in age. Shale makes up the majority of the lithology, and there are also some sand deposits. The depth of the well's thickness is 410.71 meters.

2.4.2 Lower Goru Formation

There is a depositional gap of 30Ma between early Cretaceous Lower Goru and Sembar Formation of Jurassic age. It consists further four members namely classified as A, B, C, and D succession of sand bodies.

2.4.2.1 B interval Lower Goru Formation

B Interval Lower Cretaceous B interval is sands and shale.

2.4.2.2 A Interval Lower Cretaceous

A sand interval of Lower Goru is also well-known as “Massive Sand” considered to have pure sands. The thickness of A interval encountered in study well is 20.9meters. B Interval Lower Cretaceous B interval is sands and shale. The thickness encountered in well is 175.98meters.

2.4.2.3 C Interval

The C interval, often referred to as the Middle Sand interval of Lower Goru, dates from the Low Cretaceous Period. Shale makes up the lower portion of the C interval, and sand makes up the higher portion. The C interval has a thickness of 143.98 meters.

2.4.2.4 D interval

Upper sand is another name for the Lower Goru D period, which is also shale-rich.

2.4.2.5 Shale interval

The Lower Goru Formation's shale interval is found above the D interval. The depth of the well's thickness is 585.27 meters.

2.4.3 Upper Goru Formation

Upper Goru Formation is of late Cretaceous age having thickness of 278.10 in well. It contains shale which acts as regional top seal.

2.4.4 Ranikot Formation

Ranikot is of Paleocene age having thickness of 929.93meters in well. It contains sandstones with interbedded shale. Sui Limestone is of Eocene age having thickness of 194meters.Limestone is major lithology along with interbedded shale.

2.4.5 Ghazij Formation

Ghazij Formation is of Eocene age it provides regions top seal in entire Basin mainly consists of shale. Thickness of Ghazij encountered in well is 696meters.

2.4.6 Kirthar Formation

Kirthar Formation is of Middle Eocene to Early Oligocene is divided into four members mainly consists of Limestone, Sandstone, Shale, and Marl (Kazmi and Jan 1997).

2.4.7 Habib Rahi Habib

Rahi Limestone is of Eocene age having thickness of 199meters in well. It contains Limestone as a major lithology.

2.4.8 Sirki Member

Sirki member of Eocene age is having thickness of 39.00m is encountered in this well. It is the second member of Kirthar Formation.

2.4.9 Pirkoh Formation

Pirkoh member of Eocene age is having a thickness of 51m is encountered in this well. It is the oldest Member of Kirthar Formation.

2.5 Petroleum system of Gambat block

The petroleum system must contain an active source rock as well as all crucial components and processes required for the accumulation of oil and gas. These components comprise the source, overburden rocks are may be seal rocks, reservoir rocks, and rocks. The production of the trap, its movement, and the accumulation of the petroleum are necessary steps. For petroleum accumulation to take place, each of the aforementioned factors and processes must be present both in time and space (Magoon & Dow., 1994).

1. Source Organic Rich shale of early Cretaceous inside Sembar Formation containing Type III Kerogen and TOC >1% is the proven source rock in the area (Qadri and Shuaib, 1986).

2. Reservoir Basal, Massive, and Middle Sands of Lower Goru act as a reservoir in the study area. They act as reservoir as well as cap rock for sands lies below them (Baig et al., 2016).

3. Seal Upper Goru act as seal for Lower Goru sands in the study area while Ghazij shale also act as seal for Eocene Sui Main Limestone in the surrounding areas (Ehsan et al, 2018).

4 Trapping Mechanism The area with presence of both structural (Horst Structures) and Stratigraphic (pinch outs) traps. Presence of both traps makes it a potential candidate for hydrocarbon presence.

CHAPTER 3
SEISMIC DATA INTERPRETATION

3.1 Introduction

Interpretation of seismic data includes different steps to resolve the seismic section and its stratigraphic and structural sequences. The main objective is to locate and set a point or area for the hydrocarbon that is trapped in a structure. These seismic sections basically have the information of the subsurface response due the different artificial waves through which we have produced the seismic waves (Zhou, 2014).

3.2 Approaches to Seismic Interpretation

The aim of the thesis is to identify the delineation of subsurface structural features upon which the well was drilled. Basically, there are two main approaches to analyze seismic data; Stratigraphic correlation and Structural correlation.

3.2.1 Stratigraphic Analysis

Stratigraphic analysis encompasses interpretation of genetically related sedimentary sequences which characterize variations in the sedimentary depositional environments. Unconformities are marked by drainage pattern which gives direct information about depositional environment. Lenses, reef, unconformity are examples of strati graphical trap (Sheriff, 1999).

3.2.2 Structural Analysis

Structural approach visualizes the potential structures that can withhold hydrocarbons and thus an integral part in the petroleum plays of the region, commonly known as “Structural Traps”. We have applied the structural technique. Structural interpretation is done by the help of seismic data (Morton & Woods, 1993).

3.3 Base map preparation of research area:

Orientation of seismic lines in the surveyed area are displayed by the help of base map. It contains wells, shot points, and Seg-Y data containing latitude and longitude. Using the navigation data base map can be prepared as we ca see in figure 3.1.

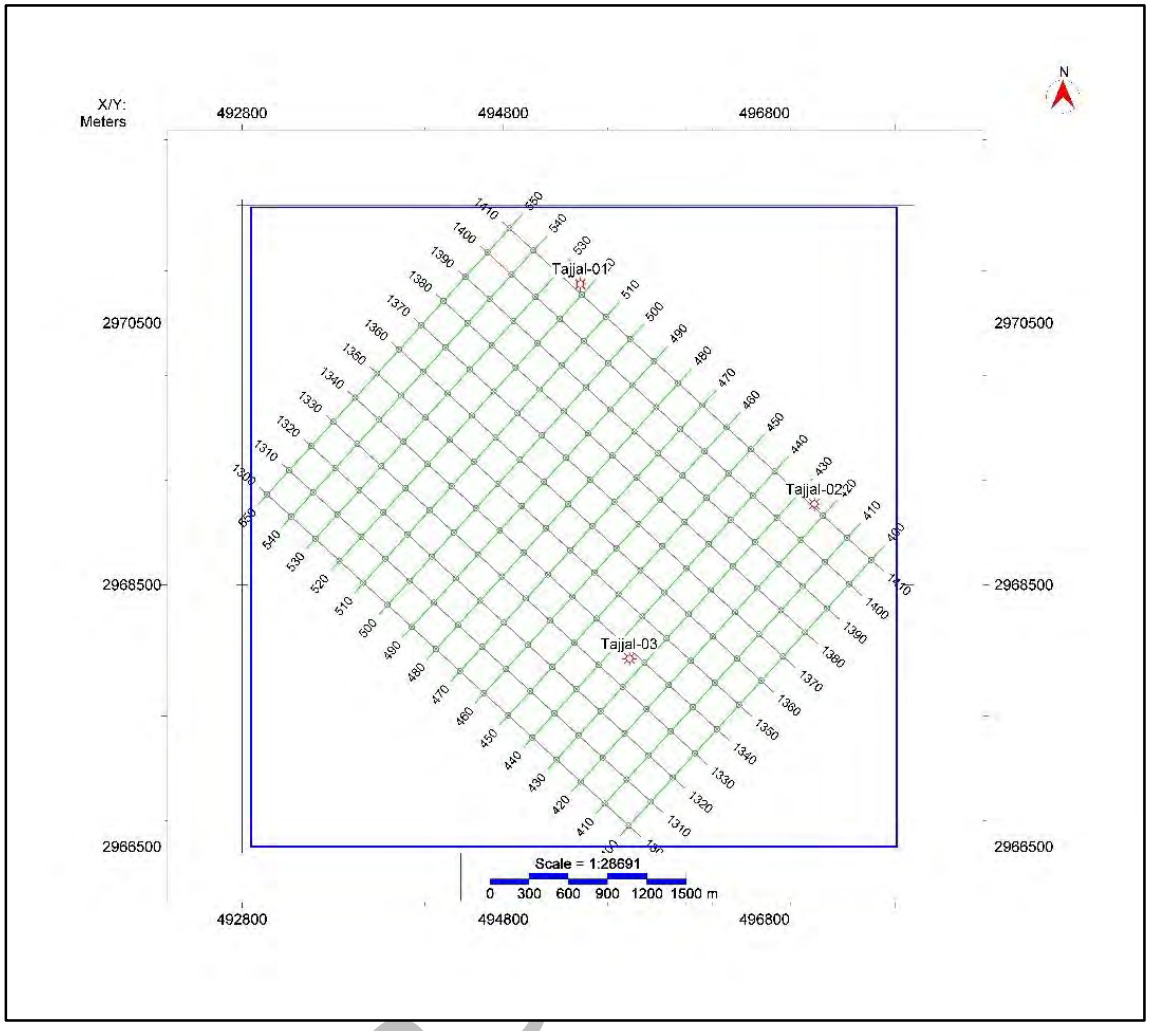

Figure 3.1 Representing the base map of the area

3.4 Synthetic seismogram

Synthetic seismogram was generated by correlating seismic data with well log data of required well. In the seismic interpretation synthetic seismogram is a direct 1-D modeling. (Ganley, 1981). As there is direct relation between seismic reflection pattern and lithology observed, so in this regard synthetic seismogram is most helpful in linking seismic section with geology (Cooper, etal., 2004). Velocity obtained from DT log and density from RHOB log has been incorporated to generate synthetic seismic trace. This generated trace was nearly related with seismic trace from any seismic line which is nearer to the well containing all the logs. Synthetic seismogram of Gambat area is shown in (Figure 3.2). Synthetic seismogram is correlated with the seismic data (time domain) at well location that is in depth domain.

The interpolation (Tie) of well log data and seismic data gives a good correlation.

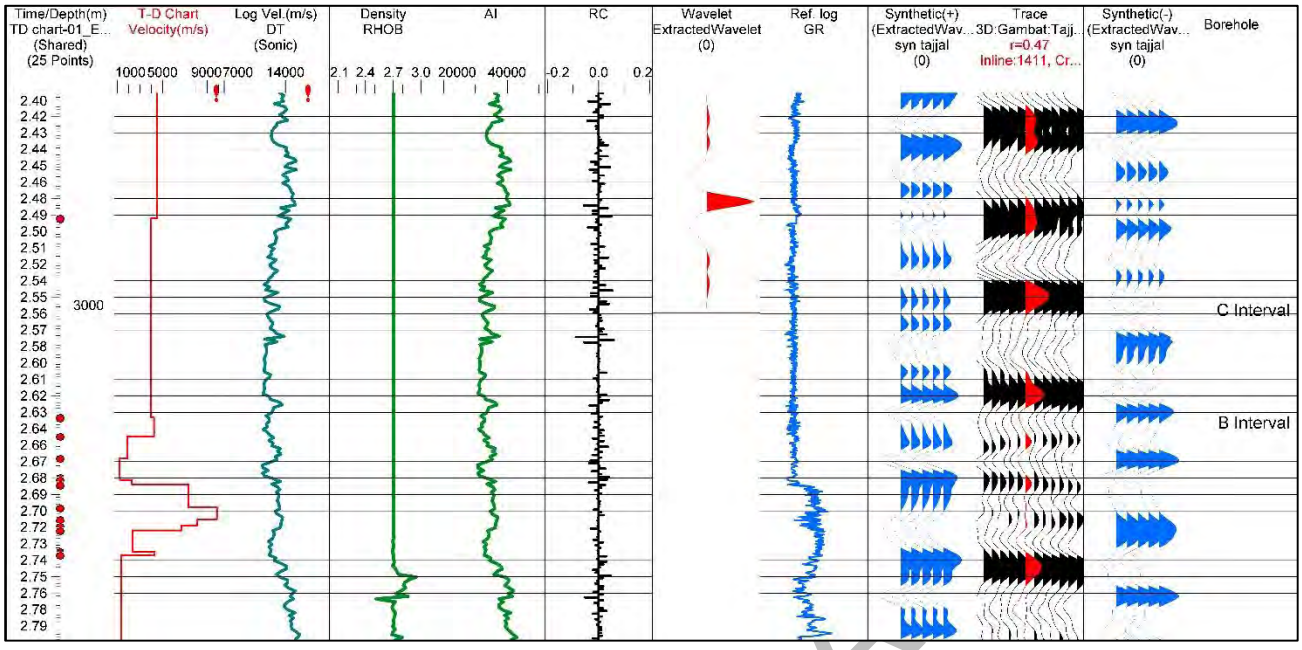

Figure 3.2: Representing the synthetic seismogram through which well to seismic tie was done.

3.5 Demarcation of Horizons of Interest:

Synthetic seismogram is used to mark the structural and physical characteristics of horizons of interest in the study area (Ali et al., 2019). Because it allows the identification of the events from the well log data and relates them with seismic reflections to get an idea about the polarity of seismic data (Kearey, 2009). The top and bottom of horizons are picked over the whole 3D data volume, after seismic to well tie. Figure 3.3 shows the marked horizons of interest which are lower Goru and B interval. In this study area there is normal faulting. Marking horizons 2 horizons have been marked and interpreted on the seismic lines of Gambat area, which are as follow

1. Lower Goru Formation
2. B Interval
3. C Interval

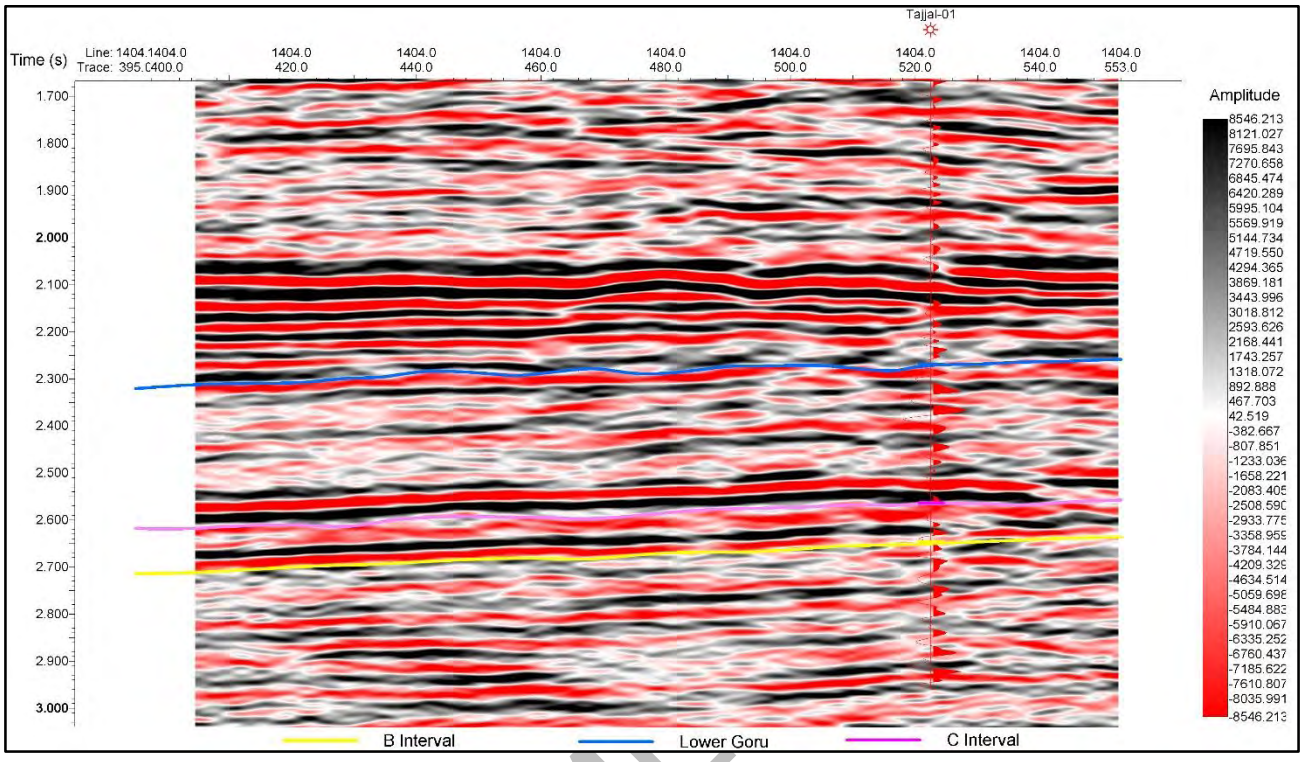

Figure 3.3: Representing the marked horizon on the Seismic section.

3.6 Marking of faults

The discontinuity in strata at certain locations helped in identifying faults. As faults form a variety of traps for accumulation of hydrocarbons; delineating them is the major and foremost concern of an interpreter. Seismic time sections the time section clarifies the subsurface picture of the horizons (TWT on Yaxis) against the shot points (on X-axis), as observed on the seismic sections. From the seismic section time of each reflector is marked and plotted it against the shot points F1 fault is marked as shown in (Figure 3.4).

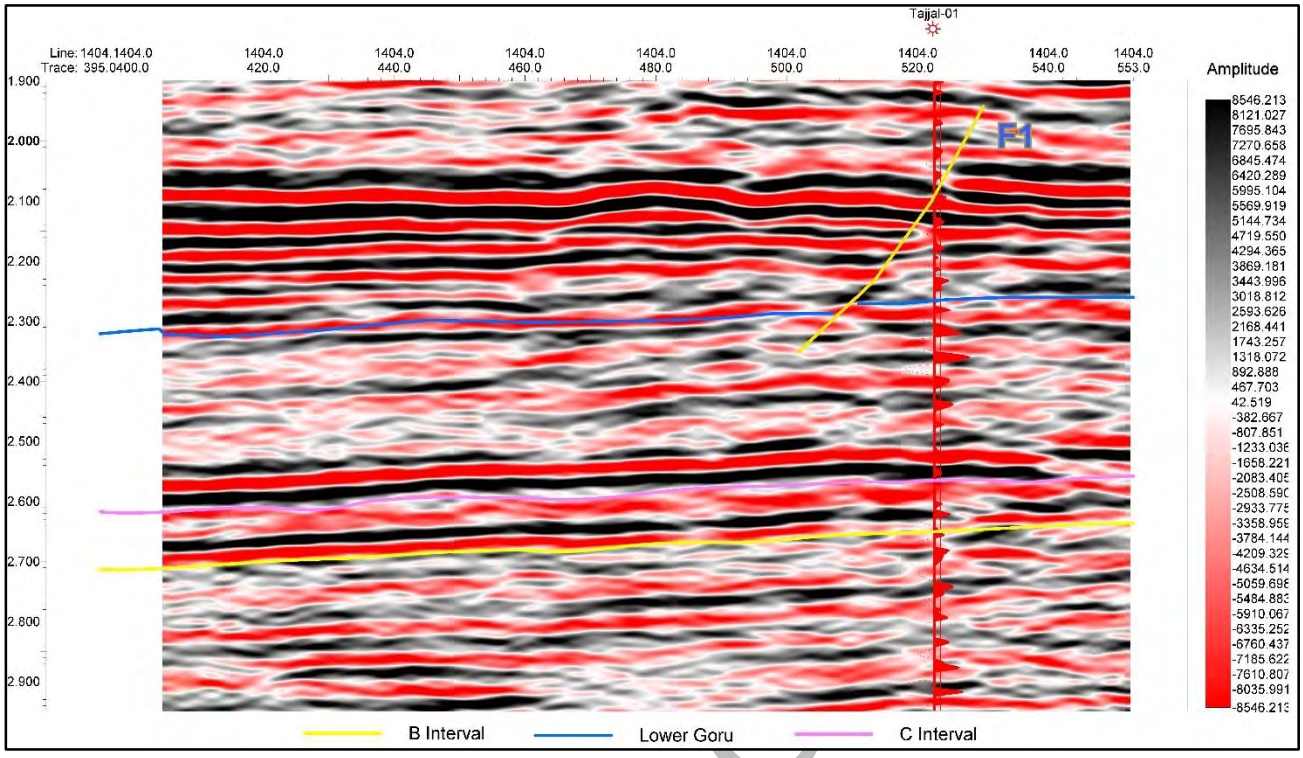

Figure 3.4: Representing the seismic section along with Normal Fault marked F1

3.7 Grid Formation

Grid is basically the extrapolation of seismic data, among the seismic lines where the data is not acquired. To see variations in time and depth in given 3D cube, a grid is developed for these geophysical quantities by digitizing the time slice on the base map. Different colors of the grid show time variation in the data that is in time domain and depth domain. Different color in the Color bar dhow that the horizon is somewhere deep and shallow.

3.8 Contour map generation

The contour map generation is the final result of seismic interpretation on which the entire process is depends upon. So, after gridding, variations in the time and depth are needed to be observe in a specific time and depth interval. Which is done by making contours on that section. They join the points of equal time and depth as given in 3D cube (Coffeen, 1986). Also, the contour maps show any structural trend of faulting and folding in that particular region.

3.8.1 Depth Contour map

These contour maps are created using the values for depth at specific points. These show the depth variation of horizons in the subsurface.

The interpretation of a depth contour map is the same as that of a time contour map, with the exception that the units for a depth contour are meters rather than milliseconds, and depth is now shown instead of time.

3.8.1.1 B interval Depth Contour Map

Depth contour map of B interval shows 3D variation usually with respect to depth displayed over the base map which indicates the lateral variation of the formation in the subsurface. Red to green color represents shallow part of the formation and blue color represents deeper part. We usually consider shallower part as producing because it is area of low over pressure. The shallowest part (white to yellow color) of the B interval is prone to oil and gas in the study area as it represents the low-pressure area because of low overburden as compared to its deepest part (blue color) as shown in (Figure 3.5). B interval is composed of Sand and shale beds. Depth contour map of B interval shows the 3D variation in depth. We generally conclude that where there are low contour values it is hydrocarbon bearing zone.

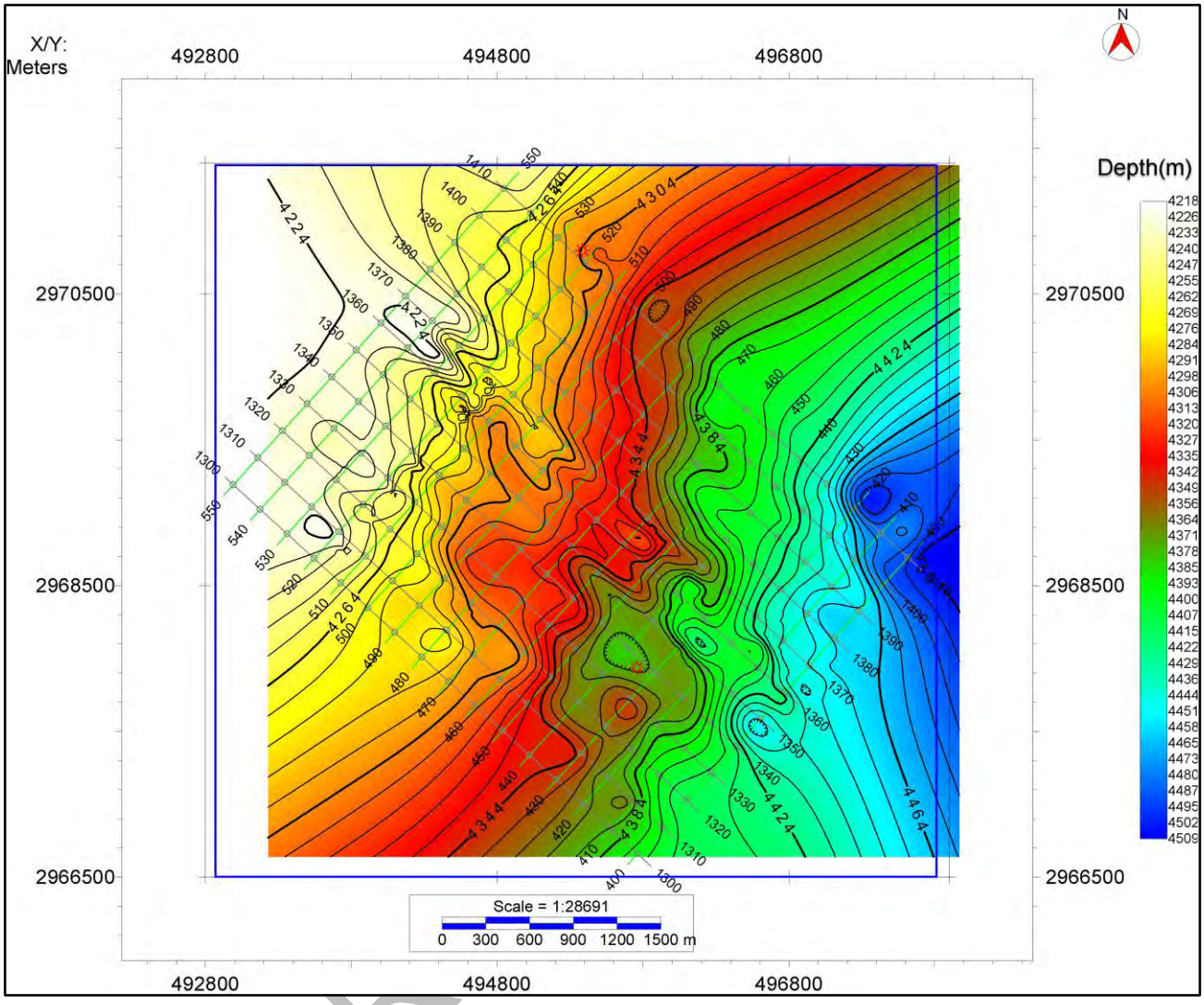

Figure 3.5: B interval Depth contour map having contour interval of 8m deep along eastern side.

3.8.1.2 C interval Depth Contour Map

The contours were generated by using Kingdom software. Contour interval is 10m for C interval. The NE portion of the map shows that the formation is lying at much deeper depth, as compared to the SW portion where it is shallower. As we move towards the west of the study area, the depth of C interval Decreases (Figure 3.6).

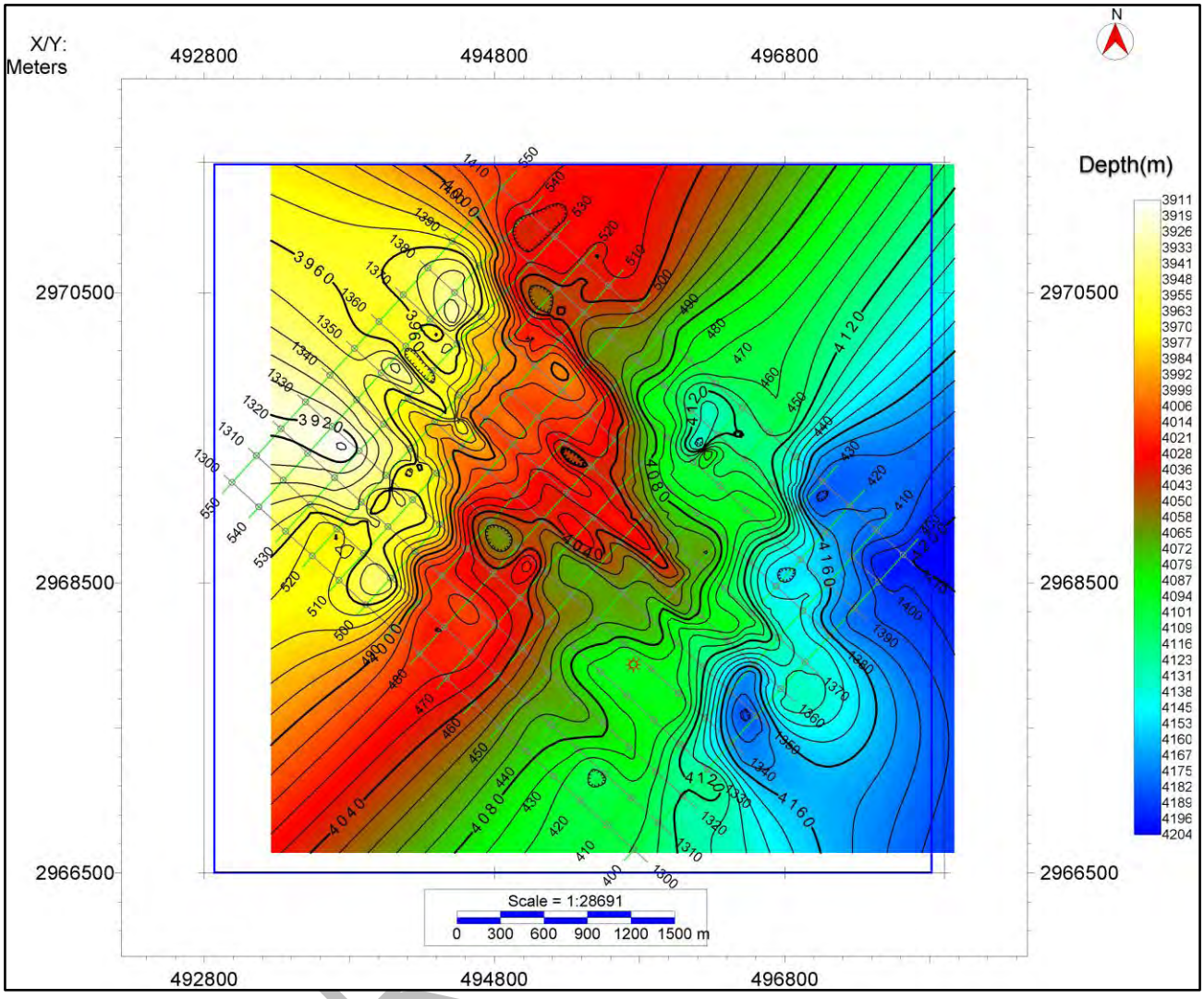

Figure 3.6: C interval Depth contour map having contour interval of 10m deep along eastern side.

3.8.1.3 Depth Contour Map of Lower Goru Formation

The contours were generated by using Kingdom software. Contour interval is 8m for Lower Goru Formation. This formation mainly comprised of sand. The contours were generated by using Kingdom software. Contour interval is 10m for Lower Goru Formation. For which the Lower Goru formation is lying at shallower depth i.e., approximately 2389. As we move towards the east of the study wells, normal faults encountered which shows the Lower Goru formation is lying at higher depth reaches highest depth of about 2481 meters as in (Figure 3.7).

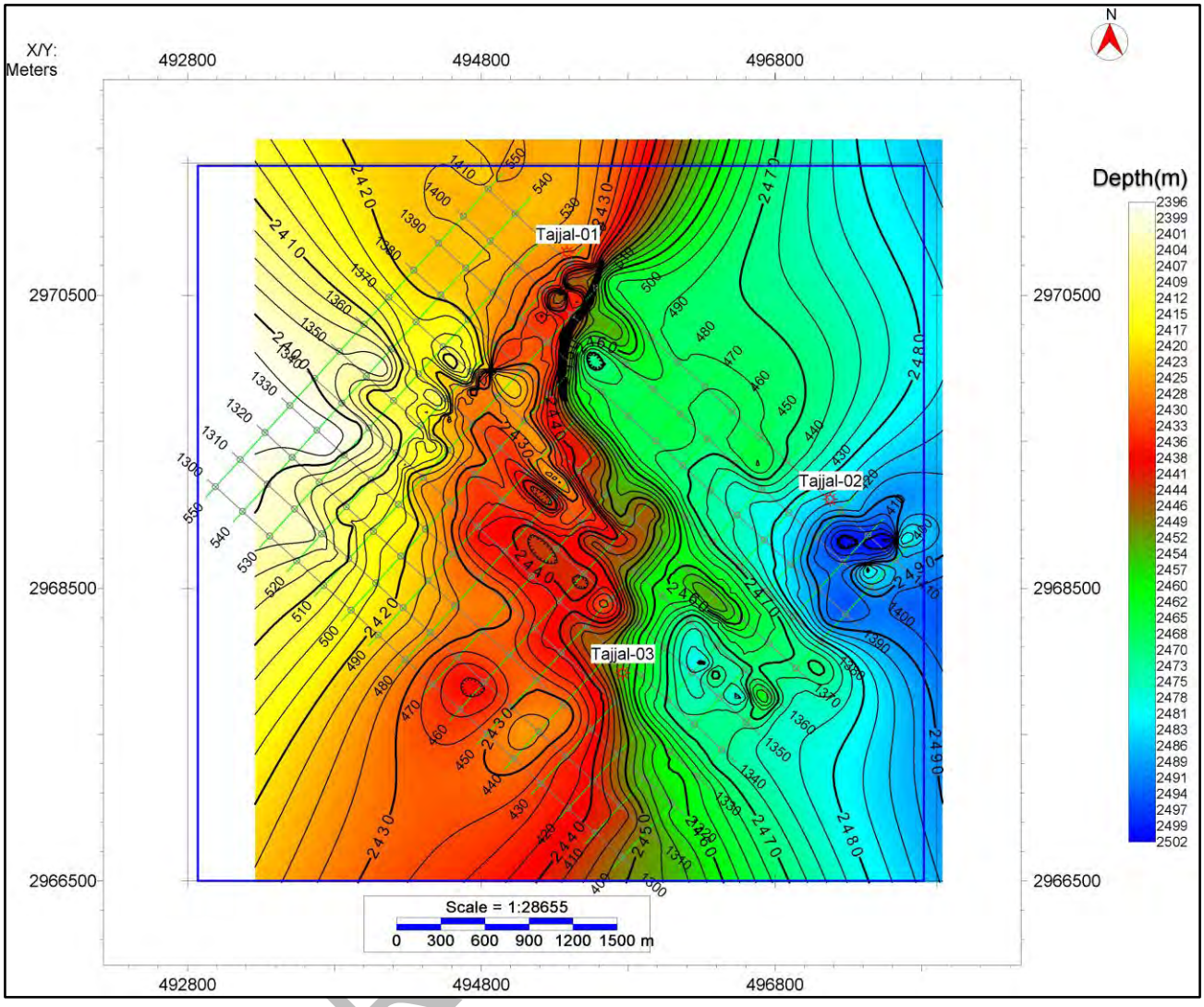

Figure 3.7: Lower Goru Formation depth contour map deepen along eastern side

3.8.2 Time contour Map

TWT contours show contours with same time values. These numbers depict the amount of time it takes for a seismic wave to leave its source, travel through the earth, hit a reflector, and finally return to the surface. These are displayed on a base map along with the latitude and longitude information for each shot point. For TWT contour mapping, a time grid is created for each horizon that displays the marked horizon time using various colors.

3.8.2.1 Time contour map of B interval

The contours were generated by using Kingdom software. Contour interval is 0.025 sec for B interval. By forming contour of time lateral alteration in the Formation in the subsurface. The NE portion of the map shows that the formation is lying at much less time, around 2.625 seconds, as compared to the

SW portion where it is at higher time i.e., approximately 2.719 seconds. As we move towards the west of the study well, the B interval time decreases (Figure 3.8)

Figure 3

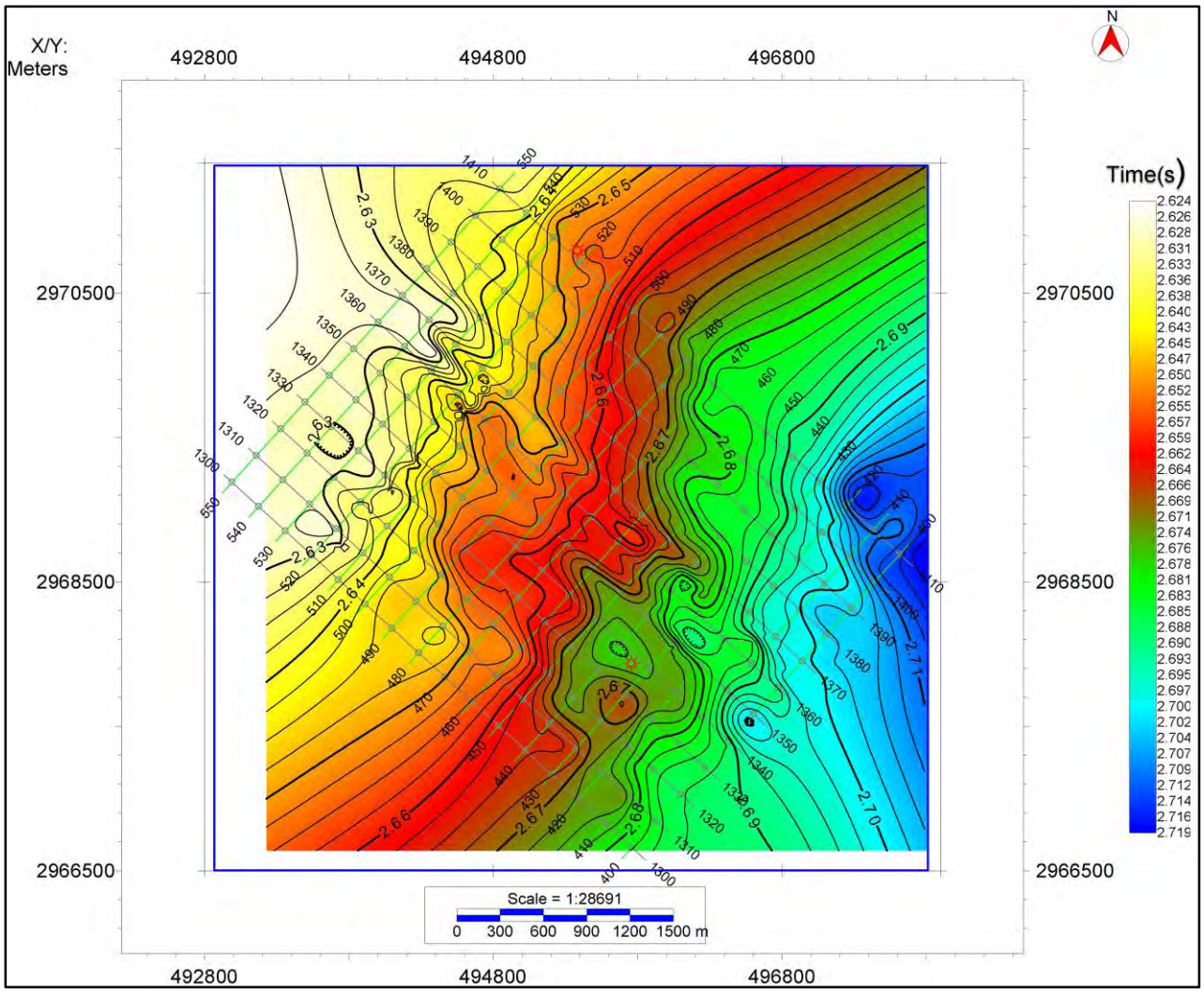

.

Figure 3.8: Time contour map of B interval deepen along eastern side with blue color

3.8.2.2 Time contour Map of C interval

The time contour map of C interval indicating a map which shows a 3D (X, Y, and Time) pattern showing the fluctuation in time on the base map to represents the lateral continuity of C interval in the subsurface as shown in the figure 3.9. In this Figure the white to red color is reflecting the shallowest part of the formation whereas green to blue colored part is an indicator of the deeper zones. The color bar

(Figure 3.9) clearly shows an synclinal geometry.

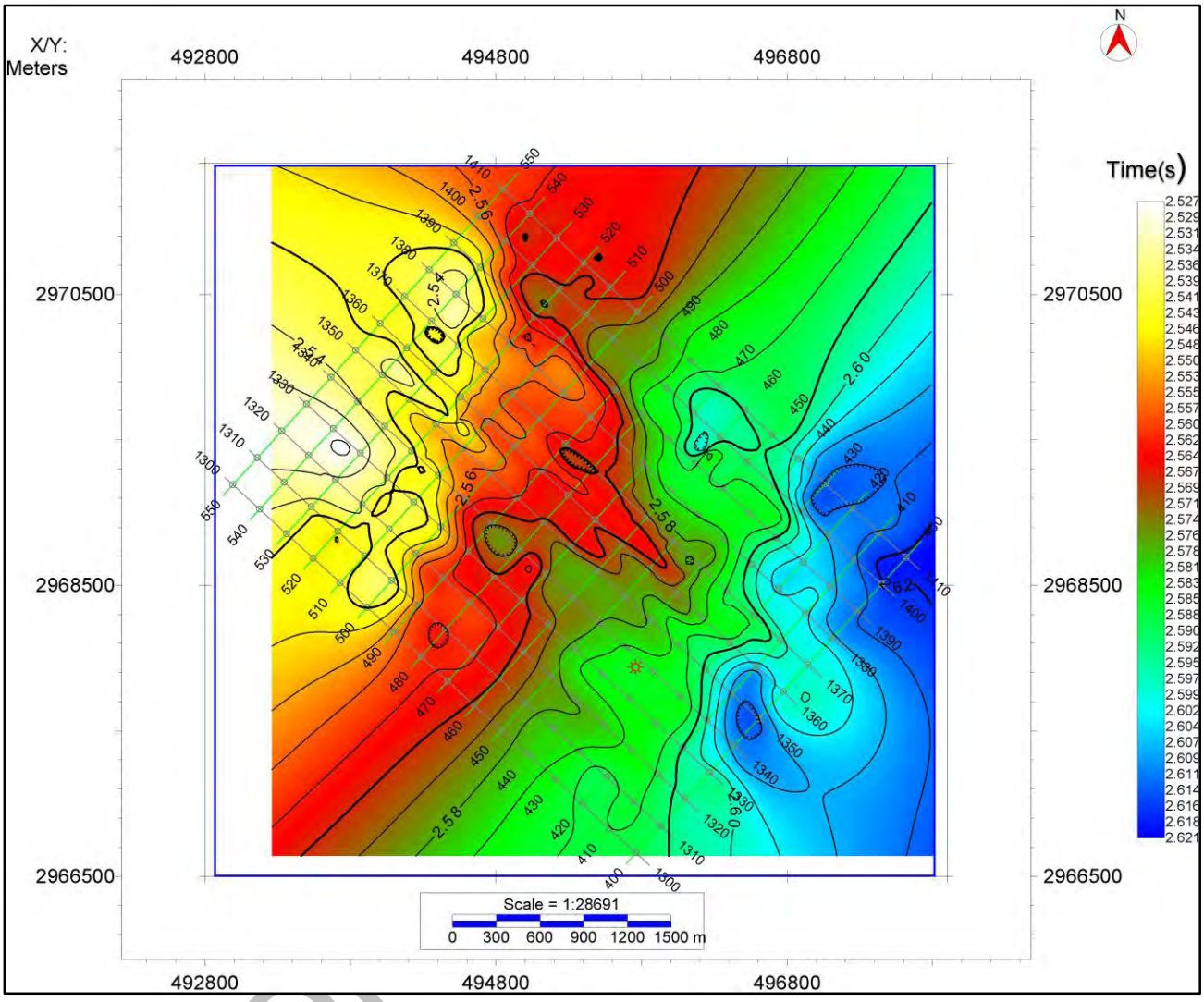

Figure 3.9: Time contour map of C interval deepen along eastern side with blue color

3.8.2.3 Lower Goru Formation Time Contour Map

The time contour map of Lower Goru Formation indicating a map which shows a 3D (X, Y, and Time) pattern showing the fluctuation in time on the base map to represents the lateral continuity of the lower Goru Formation in the subsurface (Figure 4.10). In this figure the white to yellow color reflect the shallowest part of the formation whereas the blue colored part indicates the deepest zone. As shown in (Figure 3.10) the time contour map of Lower Goru Formation is deeper in eastern side as compared to western side.

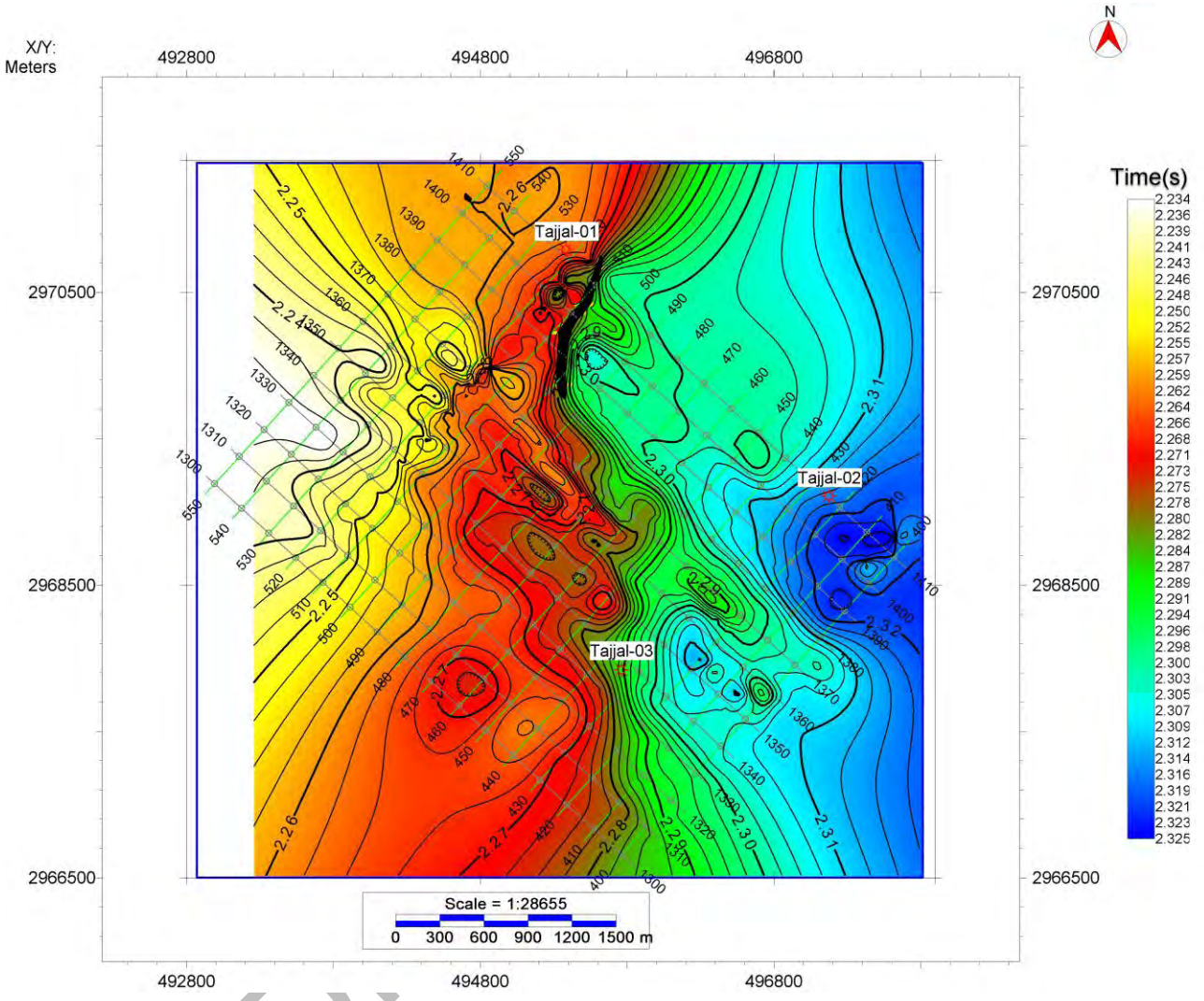

Figure 3.10: Lower Goru Time contour map showing that contours are deepen along eastern side with blue color

CHAPTER 4
PETROPHYSICS

4.1 Introduction of Petro physics

For hydrocarbon exploration, Petro physical analysis is performed to characterize reservoir properties and their relationships with fluids such as oil, gas, and water. (Tiab& Donaldson, 2004). Wire-line log data in the form of well logs, which include a wealth of information on the reservoirs, is used for this purpose. (Cosgrove et al., 1998). The term "petrophysics" is proposed to describe the physics of specific rock types. (Archie et al., 1950). The primary goal of analysis of well log is to transform raw petrophysical data from a borehole into predicted reservoir parameters and fluid properties. (Asquith et al., 2016). It bridges the gap between core and seismic data by providing reservoir metrics like shale/clay volume, porosity, permeability, and fluid saturation, which can be used to distinguish between producing and non-producing zones. Logs, poor drilling conditions, temperature, pressure, and salinity, on the other hand, might have a negative impact on Petro physical analysis. (Azeem et al., 2016).

4.2 Important parameters for Petro physical Analysis.

For evaluation of source and reservoir characterization in Tajjal 01 Petro physics analysis are implemented. For this well log data of Tajjal-01 is used. Logs used for Petro physical analysis are Neutron log, Gamma ray log (GR) shallow resistivity log (LLS), Spontaneous potential (SP), Latero log deep (LLD), Sonic log.

The following properties are calculated from these logs. • Volume of Shale (Vsh). • Effective porosity (PHIE).

- Total Porosity (PHIE).
- Saturation of water (Sw).
- Saturation of Hydrocarbon (Hs).

For calculation of above mentioned Petro physical properties logs are classify in different tracks mentioned below.

4.2.1 Lithology logs.

In lithology track the following three logs area used

1. Caliper Log (CALI)
2. Gamma ray log (GR)
3. Spontaneous potential log (SP)

4.2.2 Caliper Log:

Caliper log use to measure the borehole size. This log gives us help to identify the cavity washouts and break outs (Bjorlykke et al., 2010). Hence this log is also called the quality check for other logs. Because if any where there is say wash out then in front of the wash out the porosity and resistivity log will not give the correct reading. Hence caliper log is very important in Petro physical analysis.

4.2.3 Gamma ray Log

The Gamma ray log is used to measure the rock unit's radioactivity. The radioactive eliminates from naturally occurring Thorium (Th), Uranium (U), and Potassium (K) present mostly in fine grain rocks. The bulk gamma ray log measures the combined response of the different radioactive elements (three elements U, Th, and K), while the spectral-gamma ray (SGR) log records the response of each individual radioactive element. A GR log measures the radiation in unit of "counts" or API and is always a positive value that gives the information about different types of lithology's. The interpretation of the GR log is based-on the lows and highs of the count rates of radiations, usually associated with "clean and clayey" lithology's respectively. It means a rock formation having more fine-grained material e.g., clay or shale indicates a relatively high GR values than that from sand/limestone. (Schlumberger, 1974).

4.2.4 Spontaneous potential log

The oldest logging measurements ever recorded is Spontaneous-Potential log which provides information that demarcate reservoir and non-reservoir rocks unit lithology in the subsurface of the sedimentary cover of earth's upper crust. Fine-grained formations e.g., clay

and/or shale have very low permeability resulting in the no current flows and thus have low SP values. In comparison, permeable and course-grained rock e.g., Sandstone, Limestone, and Dolomite have high SP values. SP log is therefore a useful measure of the rocks that can detect the permeable beds, bed boundaries, and also used in calculation of water resistivity (Schlumberger, 1974). SP log has the following advantages. (Daniel, 2003)

1. To identify permeable zones (sand) and impermeable zone
2. Detect boundaries of beds
3. Determine volume of shale

4.3 Porosity Logs

The logs that are used to calculate the porosity of rocks are called porosity logs. Sonic log, Density log and Neutron density log of Maher-01 well were used to calculate the average porosity of reservoir formation. To estimate the porosity of subsurface in particular interest zone various types of logs are used in porosity track which are given bellow

1. Sonic Log
2. Density Log
3. Neutron Log

4.3.1 Sonic Log

The sonic log gives a measure of the interval transit time (Δt) of a compressional (P wave) sound wave passing through the rock strata in the subsurface. It is always recorded in microseconds per feet. Its reciprocal is equivalent to the interval velocity of the P-wave in feet per second. The DT log is both lithology as well porosity dependent (George & Gibson, 1982).

4.3.2 Density Logs:

A properly calibrated Density Log estimates the density of rock formation. When we find out density of specific matrix then porosity of the matrix can easily be calculated through this. The density log is a useful tool for lithology identification and is also helpful to give a quantitative measure of the Total-Organic Content (TOC). Density log is routinely used for the delineation of the overpressure zone and porosity estimation (Rider, 2002).

4.3.3 Neutron Log:

A Neutron Log (NPHI) gives a measure of the hydrogen index and gives direct information about pore spaces present within a rock body. It counts the slowed down neutron after its interaction with the rock units. The speed of these neutrons is slower down due to interaction with the nuclei of hydrogen atoms. As both water and hydrocarbons contain hydrogen atoms therefore NPHI provides data about hydrogen in the pores of the rock formation. The higher hydrogen atoms (e.g., in water) in pore spaces results in high NPHI value which is vice versa in case of hydrocarbon (Schlumberger, 1974).

4.4 Resistivity log:

Internal fluid's resistivity is measured using a resistivity log, which is either magnetically generated deeper into the formation or communicated directly to the rock using an electrode. (Asquith and Gibson, 2004). In resistivity track during Petro physical interpretation generally following logs are displayed,

1. Latero Log Deep (LLD).
2. Latero Log Shallow (LLS)

4.4.1 Latero log Deep (LLD):

LLD log is also known as electrode log. LLD log as compared to LLS log have larger depth of penetration. Latero log mostly incorporate in measuring salt water muds filled boreholes resistivity (Rmf). This log is used both in fresh and saline mud.

4.4.2 Latero log Shallow (LLS):

Latero log shallow (LLS), used for shallow investigation of the transition zone / invaded zone. Because the depth of the investigation is smaller than the LLD.

4.5 Marking zones of Interest criteria

Criteria used to mark the interested zones are:

(1) Stable calliper log should be used to represent the gauging of well.

(2) Display of GR log usually shows low value indicating low clay content.

(3) MSFL<LLS<LLD

(4) Crossover should be made by decreasing density and neutron curve.

(5) Sonic log (Dt) values should be on lower side.

4.6 Schematic Workflow for Petro physical analysis:

The following workfellow is used for the Petro physical analysis (figure4.1).

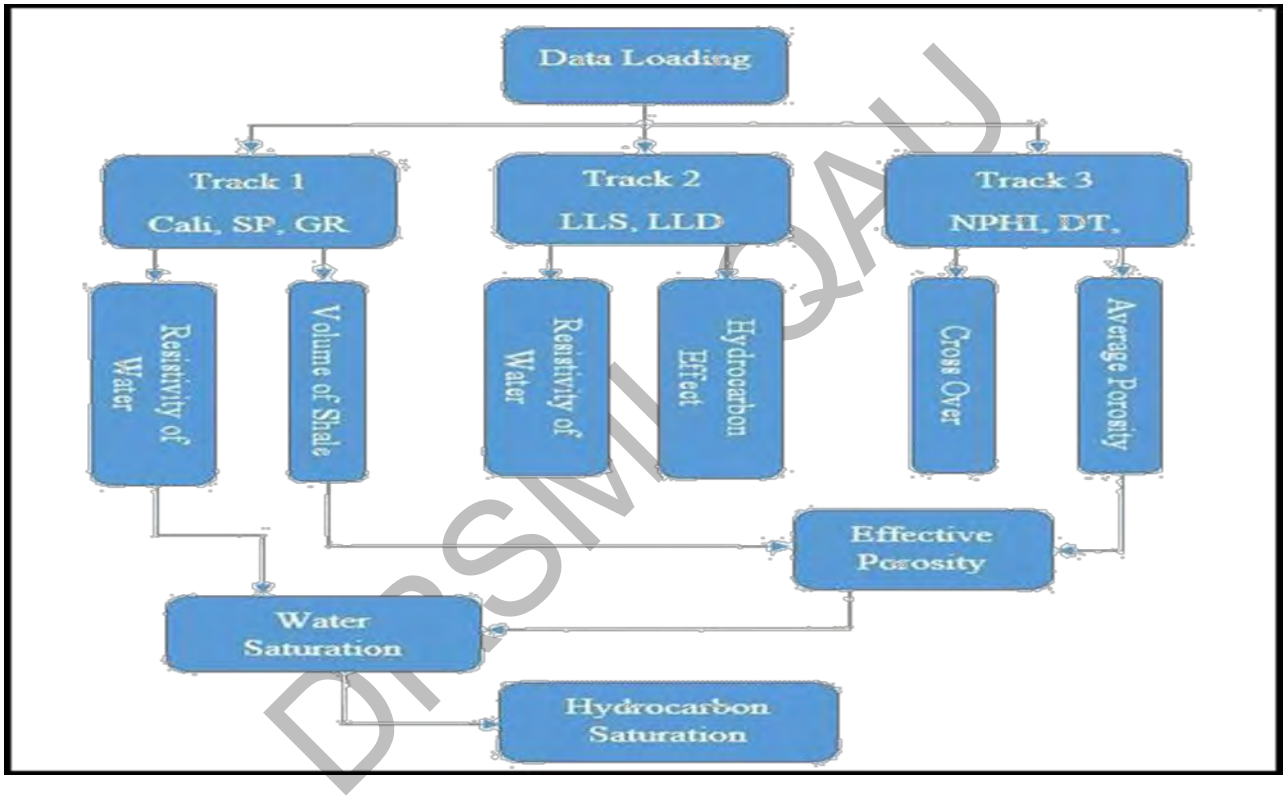

Figure 4.1: Whole Petro physical work flow used for marking zones and reservoir estimation

4.7 Shale volume measurements

Shale, Sandstone, and Carbonates are the lithology of subsurface strata. Reservoir rocks are not homogeneous, although they do have lithological interrelation to establish how clean a lithology is, the volume of shale throughout the reservoir rock is estimated. Gamma ray logs from well data are used to calculate shale volume. (Vsh) SP and GR logs are the best logs used for the measurement of shale volume in the formation from equation 4.1. In clean rocks the clay contents are less as compared to shaly or dirty rocks (Gendur, 2011).

Vshale = (GRlog - GRmin) / (GRmax - GRmin) eq 4.1

Where:

GR log = Gamma ray log for formation

GR max = Maximum GR of Shale

GR min= Min SP reading of clean formation

4.7.1 Density porosity

Formation density log can be used to estimate bulk density of the formation to measure its total porosity. It is convenient for identification of gas bearing formations. Following is the formula used for its calculations from equation 4.2:

φ= (ρma-ρb)/(ρma-ρf) eq 4.2

Where, φ = The porosity of the rock

ρma= Rock matrix density

ρb = Formation bulk density

ρf = density of fluids occupied by the porosity.

4.7.2 Neutron porosity

Porous formation can be demarcated using these logs. Hydrogen is the key element to which they respond primarily. In clean formations the quantity of the clean of liquid-filled porosity is revealed due to the filled pores. Comparison of neutron logs with other porosity logs can help in recognition of gas bearing zones. Limestone is chosen as the calibrating lithology (Gendur, 2011).

4.7.3 Sonic porosity

It is determined by using the following formula of equation 4.3

Sonic Porosity = (ΔTlog-ΔTma)/(ΔTf-ΔTma) eq 4.3

Where, $\Delta Tlog$= Time at the depth of interest

ΔTma= Matrix time

ΔTf=Time for saline or fresh water

4.7.4 Total porosity

Number of empty spaces contained in a rock formation is called the total porosity of the formation. It can be measured with the help of log measurements like neutron and density. Below given formula is used for the calculations from equation 4.4:

φT=(φN+φD)/2 eq 4.4

Where:

φT= Total Porosity

φN= Neutron Porosity

φD= Density Porosity

4.8 Estimation of saturation of water

Water saturation is the fraction of pore spaces that contain water. Which is estimated through the Archies formulae given in equation in 4.5

$$SW = \frac{\sqrt[N]{F \times Rw}}{Rt} \quad \text{eq} \qquad \text{eq 4.5}$$

here resistivity of water is Rw, True resistivity is Rt,

m is Cementation factor and n is Wettability factor

4.9 Hydrocarbon estimation:

The percentage of pore spaces that contain hydrocarbon is known as hydrocarbon saturation. The mathematical formula used to calculate the hydrocarbon saturation is given by the following equation in equation 4.6

$$Sh = 1 - Sw \qquad \text{eq} \quad 4.6$$

Where, Sh=Hydrocarbon Saturation (SH) Sw=Water Saturation (Sw).

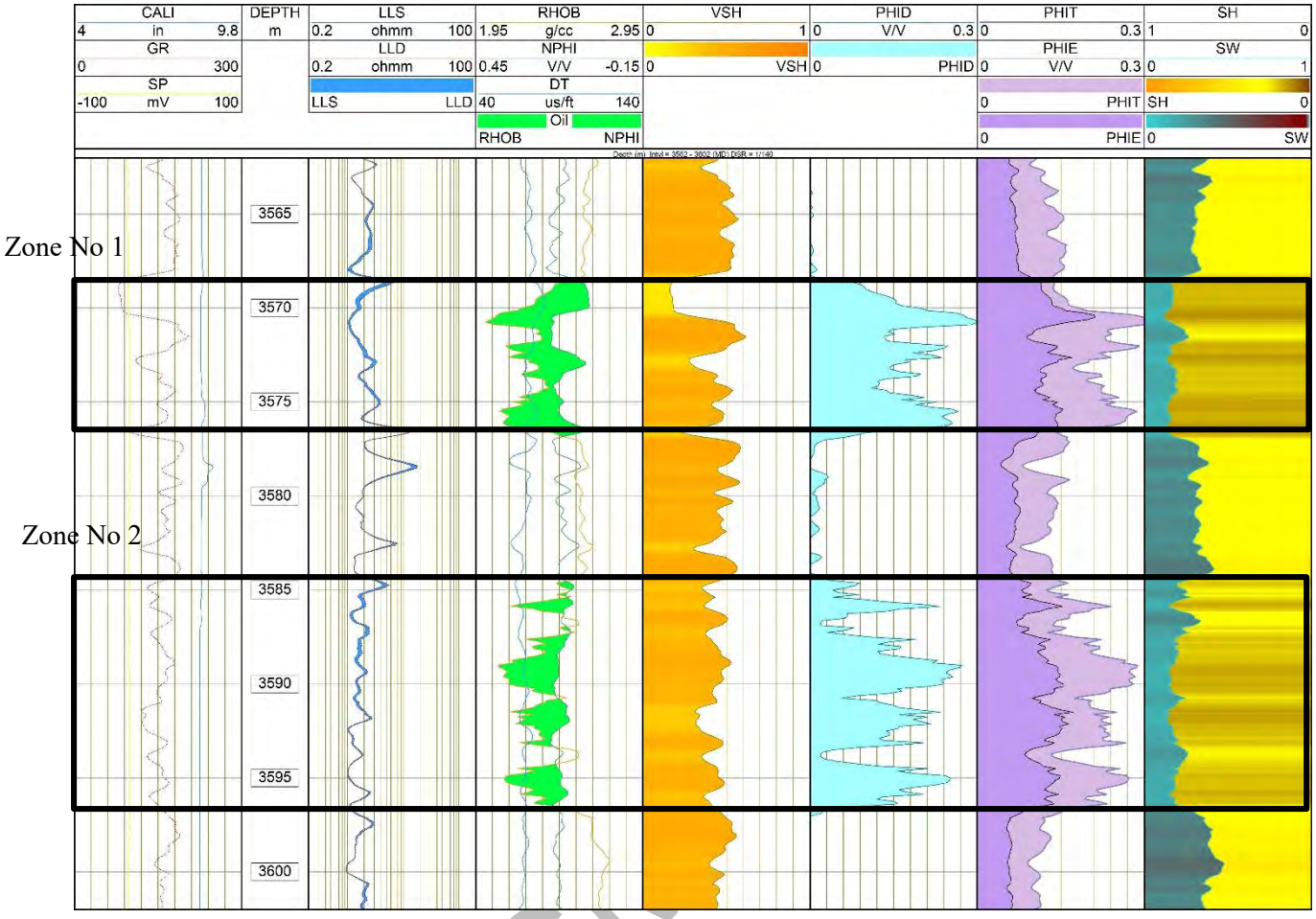

Figure 4.2: Representing the Petro physical results of Tajjal01

Table 4.1 Results of Petro physics

Zone in Tajjal 01	Depth Range (m)	Volume of shale (%)	Effective porosity (%)	Water Saturation (%)	Hydrocarbon Saturation
1	3570-3572	39.4	12.6	12.6	87.4
2	3584-3592	42	12.1	19.5	80.5

4.10 Interpretation of Well Log

For Petro physical analysis we use power log software of Tajjal 01 well. Caliper log displays stable performance with in the reservoir zone. GR values depicts the lithology existing in subsurface is shale and sand in Tajjal -01 reservoir zone, Separation of LLS and LLD is playing

very vital role as it is indicator of Fluid presence in Tajjal -01. Crossover of NPHI and RHOB is very important at the depth of reservoir zone shows fluid zone. Density porosity is calculated from density log of Tajjal-01. Petro physical interpretation of Tajjal_01 confirms that well Tajjal-01 shows presence of hydrocarbons. Tajjal_01 has 39.4% volume of shale. The effective porosity of C interval is greater than 12.6%. Water saturation ranges from 12.6%, while hydrocarbon saturation ranges from 87.4% in zone 1. Zone 2 has 42% volume of shale. The effective porosity of C interval is greater than 12.1%. Water saturation ranges from 19.5%, while hydrocarbon saturation ranges from 80.5% in zone 2 in (Figure 4.2)

CHAPTER 5

SEISMIC INVERSION

5.1 Introduction

A model of relative reflectivity at each time sample is produced via simple inversion, which may then be reversed to provide a model of relative acoustic impedance. However, a conversion to absolute acoustic impedance is necessary in order to obtain formation parameters like porosity and density. Such a conversion, however, requires frequencies close to zero hertz (Hz), which are not typically found in seismic data. An absolute acoustic impedance model can be created by combining a low frequency model acquired from borehole data with a relative acoustic impedance model created from seismic frequency range. (Barclay et al., 2008).

More information than reflector placements can be found in seismic reflection data. Amplitude of reflection is regulated by impedance. During the seismic inversion process, seismic amplitude data can be used to invert for impedance. Well data can be extrapolated to the reservoir scale via a relationship between seismic derived impedance and Petro physical variables like porosity and water saturation since the amplitude of a seismic trace is an interface property while the acoustic impedance is a layer characteristic. The best field development uses this seismic inversion approach for reservoir scale (Barclay et al., 2018). Inversion is a method of making inferences from data collected in the field by guessing, computing and comparing the definition of inversion is "it is set of mathematical procedures for, reducing the data to extract useful information about the physical world on the basis of inferences obtained from observation." (Sen, 2006). Beyond the limits of directly evaluating seismic amplitudes, acoustic impedance has proven to be a good tool for interpreting seismic data.

For the impedance contrast is large, this method is safe to use when determining target zones. It is commonly known that both the starting model and the wavelet must be carefully considered. The final inversion result will include errors in these parameters. When the reservoirs are subjected to restrictions such limited spatial resolutions, low impedance contrasts with surrounding layers, and bad data quality, more control over the inversion parameters assures good results. The low-frequency components of the seismic data were incorporated, which reduced the uncertainty in the initial model. (Gavotti et al., 2014).

5.2 Model Based Inversion

Theory Seismic inversion is the computation of earth acoustic impedance. For the quantitative interpretation of seismic data acoustic impedance is used which is a layer property. Lithology, porosity andwater saturation of the reservoir zone can be identified through impedance which has been estimated from inversion (Kneller et al., 2013).

The generalized linear inversion algorithm has been applied to a model-based inversion. With the aid of this algorithm, it will be possible to determine the seismic trace and wavelet, and it will attempt to modify or change the initial supposed or guess model. This process will be continued or repeated until the synthetic trace is the best match for the actual or seismic trace (Gavotti et al. 2014), until the error in both the synthetic and actual seismic trace is minimized. This approach is very promising for consistent model creation if you have a lot of knowledge of geology. (Kneller et al 2013). Equation 5.1 gives the basic approach of minimization of the following function which is used in this algorithm, the inversion the measure of the misfit between the seismic (real) and synthetic data (Gavotti et al., 2014).

$J = weight \times (s - w * R) + weight2 \times (M - H) * R$ Eq (5.1)

Here S = used for actual trace,

W = used for wavelet which is extracted

R = Final Reflectivity Series

M = Initial supposed/guess model

H = Integration operator convolved with final reflectivity series to produce final impedance.

In the above relation model, 1st part is actual trace and the 2nd part is supposed/guess model impedance. Modeling errors and the small amount of noise can be controlled through hard constrained (well data) additionally by the use of soft constrained (variogram model) incorporate initial guess model can be incorporated but in fact for the inversion procedure hard constrained are suggested (Gavotti, 2014). Model-based inversion work flow (Figure 5.1)

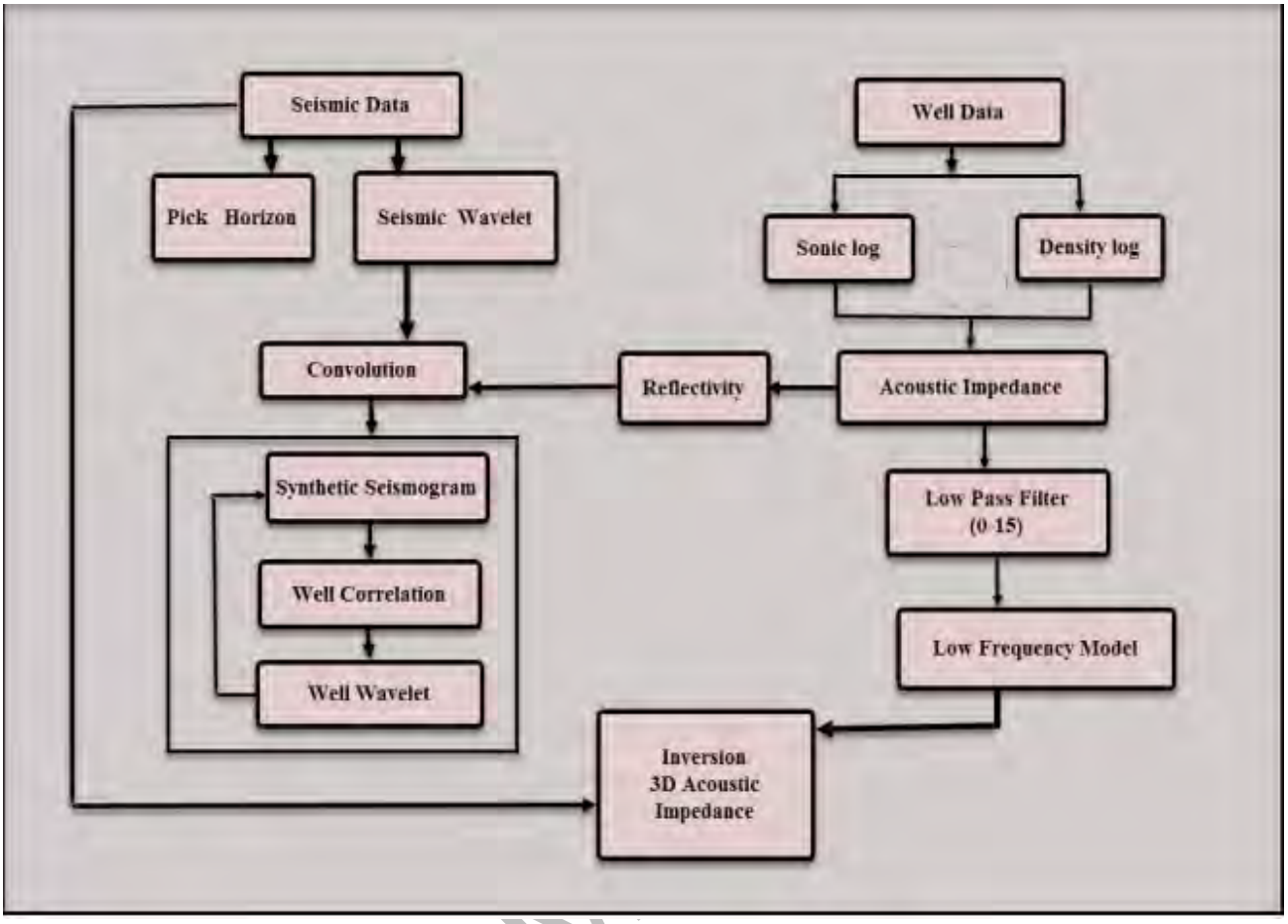

Figure 5.1: Model-Based Inversion-Based Impedance Estimation Scheme (Sen, 2006)

5.3 Extraction of wavelet:

Wavelet is very important to transfer earth reflectivity into acoustic impedance. So, extracting wavelet is better from real data then than theoretical data (Cooke and Cant, 2010). So statistical wavelet is generated from data at well location which is better to convolve with reflectivity series to compute impedance. Wavelet should be zero or minimal phase for seismic interpretation and inversion to yield an acceptable result. The degree of phase shift in the input wavelet will have a direct impact on the inversion's outcomes. According to (Jain 2013), the mistake in the resulting impedance will increase the more phase shifts there are (Figure 5.2).

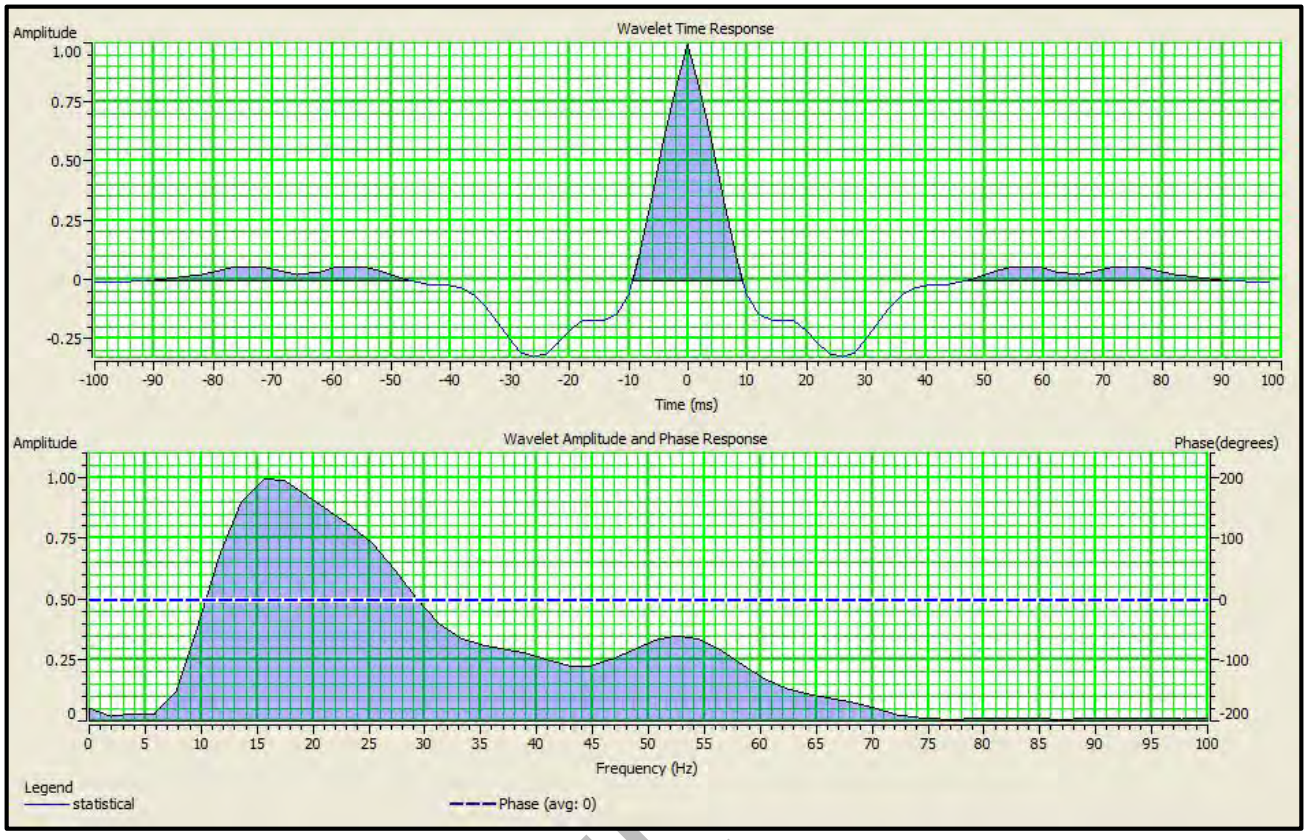

Figure 5.2: Shows an amplitude spectrum for a geostatistical wavelet created from seismic data. the dashed line showing the wavelet's average phase.

5.4 Inversion Analysis

` The given 3D seismic cube was subjected to model-based inversion for p wave and S wave following the inversion analysis at the well location. A statistical zero phase wavelet having wavelet length 20ms was extracted in time window from 2070-2270 ms for p wave and S wave as in (Figure 5.3 and 5.4). By contrasting the inverted trace at the well location with the synthetic trace, the frequency range of the extracted wavelet was modified. In Figures 5.3 and 5.4, there is a strong correlation between the synthetic (red) and seismic trace (black) is displayed. The correlation coefficient is 0.99. Between the synthetic and seismic traces, the calculated RMS error is 0.045. In (Figure 5.3), the calculated RMS error for the p impedance log was 691.134(m/s) *(g/cc), and for the S wave impedance error, it was 528.941(m/s) *(g/cc). Only the time window 2200–2700 ms, where the P wave and S wave horizons are of importance, was used for the inversion.

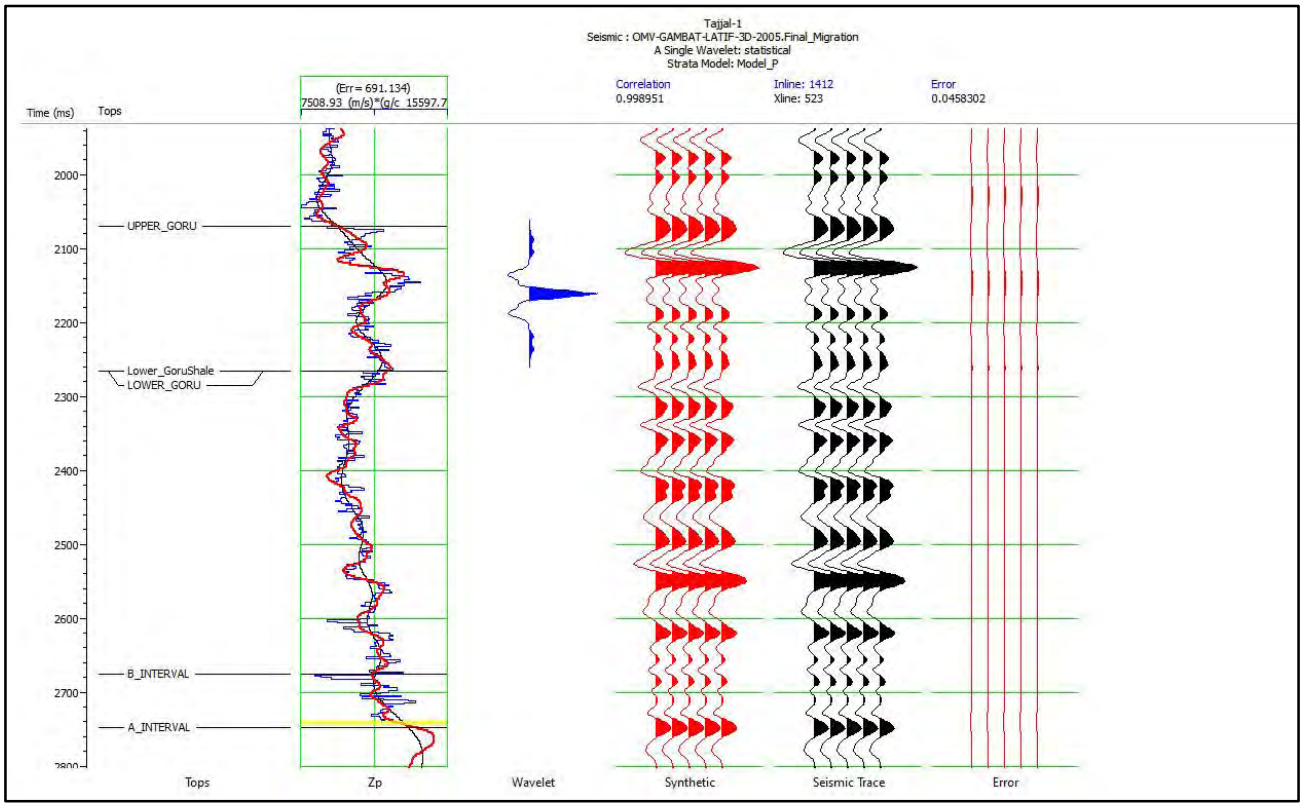

Figure 5.3: Analysis of the post stack inversion at well Tajjal 1 p wavewith initial model: (a)filtered impedance log (blue), (b) original model (black), and (red) inversion result (black).

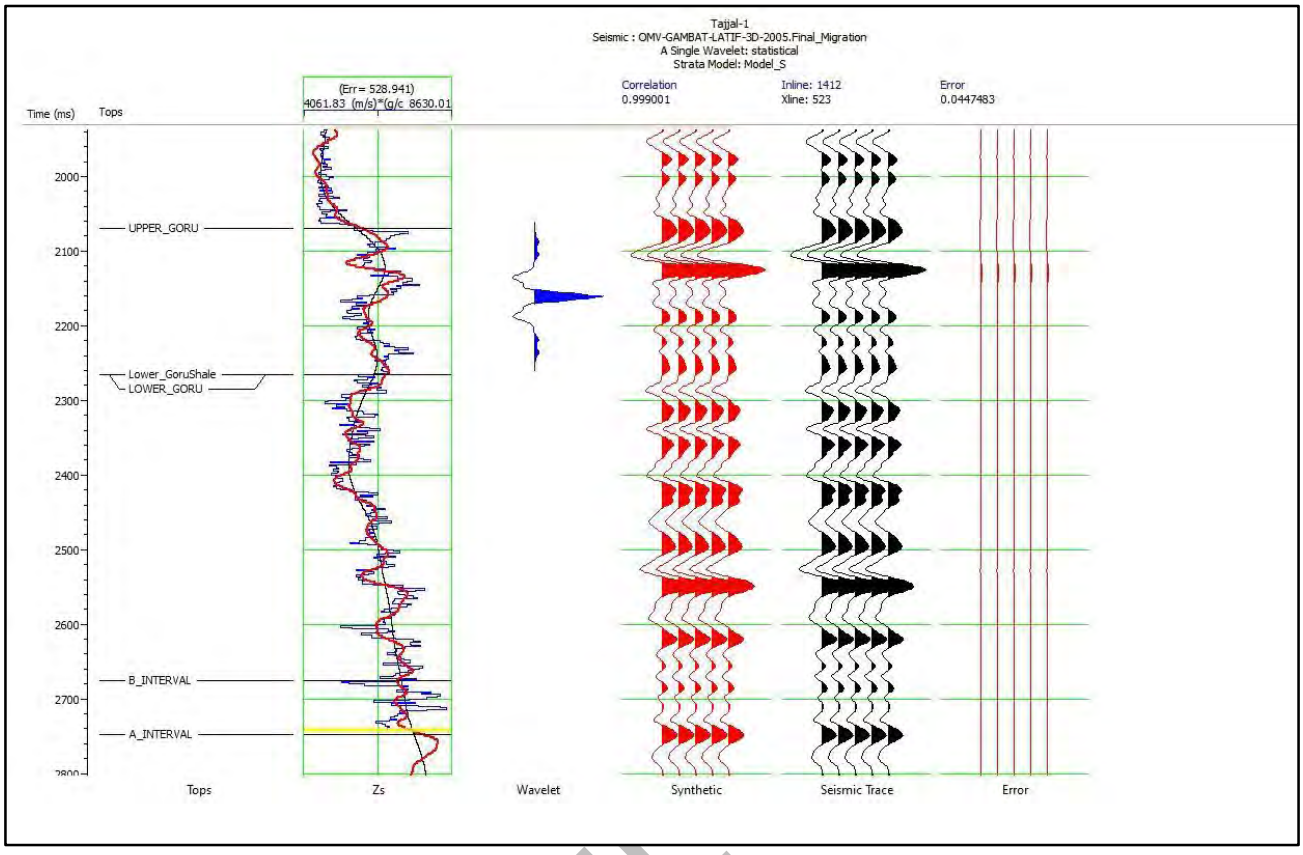

Figure 5.4: Initial model analysis of the post stack inversion at well Tajjal 01 showing impedance log (blue), initial model (black), and inversion result (red) are shown.

5.5 Correlation of Synthetic seismogram with seismic of Tajjal-01 and Tajjal-02

As in pre-inversion procedures in this work, wavelet extraction and the development of a fake seismogram were applied. Wavelet is extracted from seismic data within a specified time window, including the inline and cross line traces of seismic data cube. Wavelet which has been was convolved with reflectivity series derived from acoustic and density logs from the Tajjal-01 in order to produce a synthetic seismogram. The accompanying seismic traces at Tajjal-01 and the synthetic seismogram can be seen in (Figures 5.5). Model-based and sparse-spike-based inversions of seismic data from the Gambat region were performed.

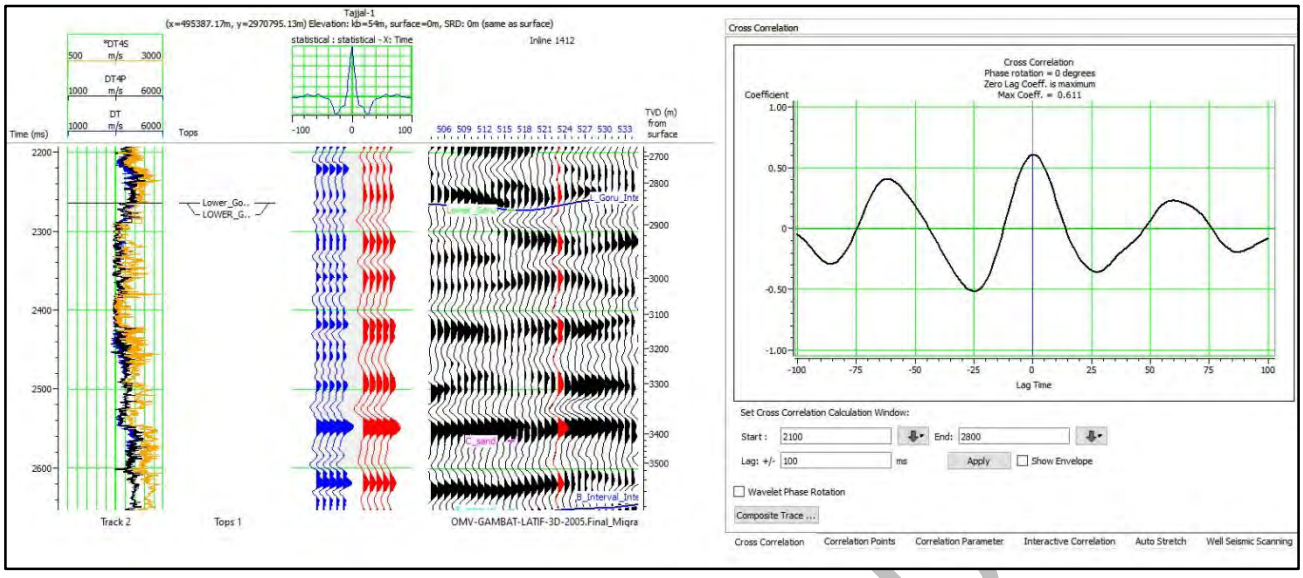

Figure 5.5: Correlation of synthetic with seismic with well along with correlation window.

5.5 Initial Model or Low frequency Model

Low frequency model is very important prospect of obtaining absolute rock properties. Low frequency spectrum is present in post stack data. During processing low frequency is removed because they come from ground roll. But in seismic inversion they are integral component. In delineation of thin bed low frequency is very important. In the absence of low frequency tuning effect is produced due to which thin beds are not resolved. By adding low frequency in initial model, the thin bed problem is resolved. (Al- Rahim et al., 2016). Adding low frequency in seismic inversion can easily calculate the acoustic impedance. Results obtained from low frequency is more reliable due to additional data input from sonic and density log, but the problem of non-uniqueness still remains in inversion. So, we made low frequency model for both the well Tajjal 1(inline 1412and Crossline point is 523) and Tajjjal 2 in which both P wave impedance and S wave impedance models are formed for both the wells with the horizons of B interval C interval and A interval (Figure 5.6, 5.7, 5.8 and 5.9). On these impedance models' different colors of bar is showing the values of impedance for both the P and S wave in (Figure 5.6, 5.7, 5.8 and 5.9). For Tajjal 1 well all of the three horizons were having low impedance for P. wave, but for the same well S wave impedance model is representing the is also low.

5.6 P wave impedance and S wave impedance for Tajjal 1 and Tajjal 2 well:

As Impedance depends upon the product of density and velocity (here p wave). In different hydrocarbon zones the response of density and velocity is different for oil gas and water. As in Tajjal 1 well at the reservoir zone of C and B interval the impedance lies at Mid-range to high of

impedance. For oil the densities and velocities along with that impedance is also slightly higher from gas response as in Tajjal well no such bearing zones are present and structurally this reservoir is not bounded by faults (Figure 5.6 and 5.8).

For S wave response as S wave didn't travel from the Hydrocarbons so where hydrocarbons are present their impedance value are low but in this case of Tajjal 1 and Tajjal 2 at the horizons of C and B interval are high and no such structural incorporation is encountered so no such zones are present (Figure 57 and 5.9).

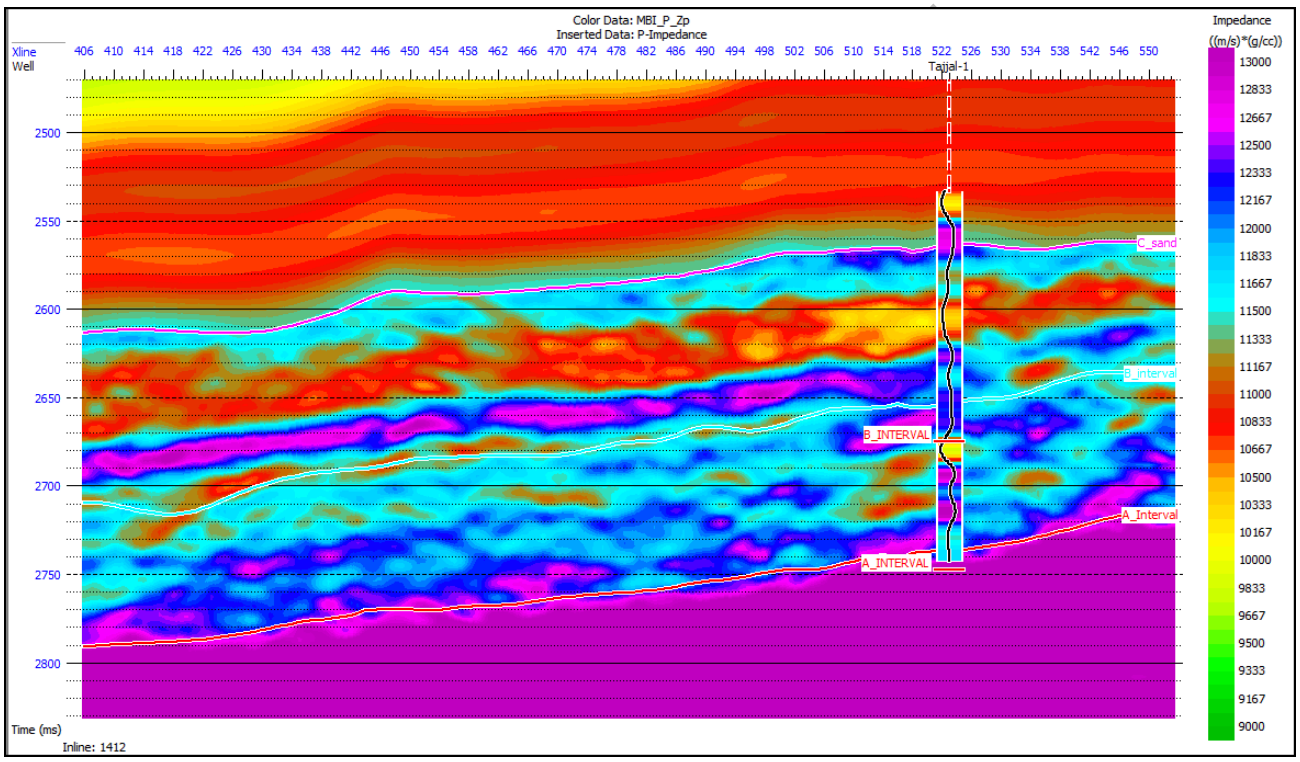

Figure 5.6: Representing the initial low impedance model for P wave of Tajjal 1 well.

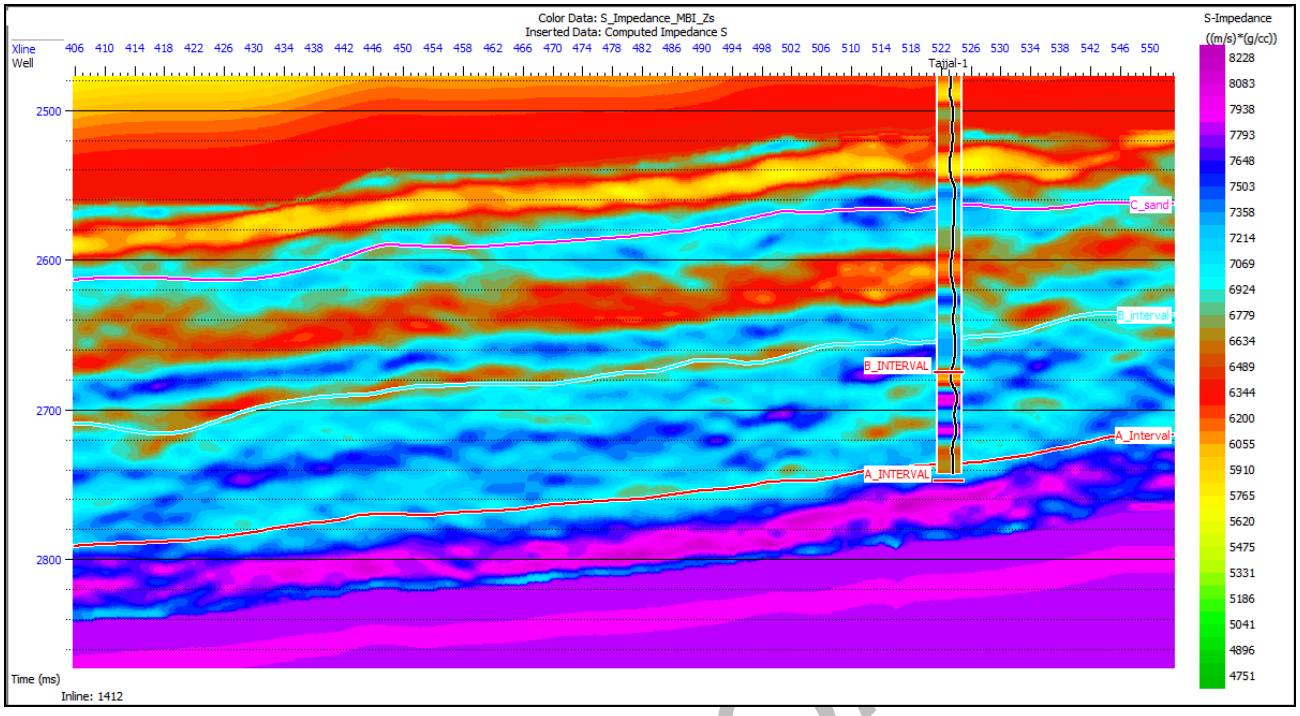

Figure 5.7: Representing the initial low impedance model for S wave of Tajjal 1 well.

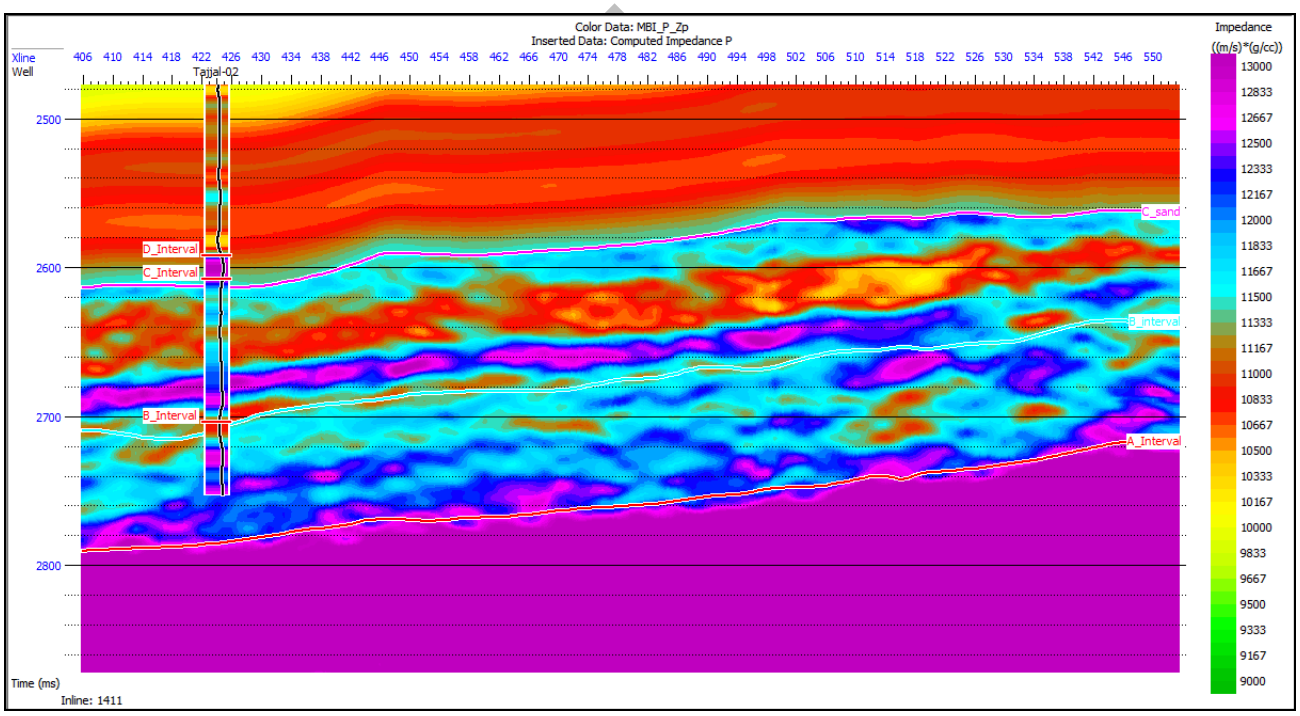

Figure 5.8: Representing the initial low impedance model for p wave of Tajjal 2 well.

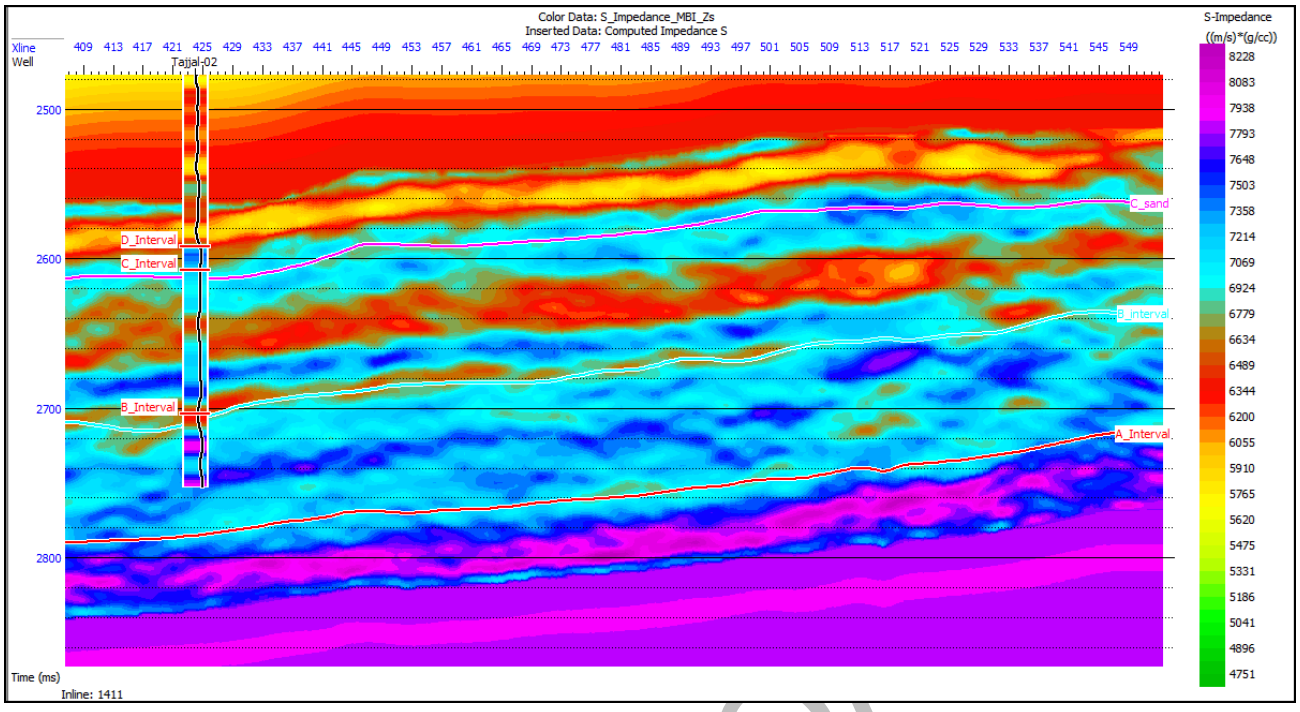

Figure 5.9: Representing the initial low impedance model for S wave of Tajjal 2 well.

5.7 Porosity Estimation

The impedance that is estimated by using model-based inversion is used for multi attributes analysis. The Effective porosity logs are selected as targeted logs. Relationship is linearly built between porosity versus P impedance as well as between porosity and the seismic attributes. The porosity is calculated by applying linear regression line. The porosity slice is shown in figure 6.10. Multi-layer attribute concluded low productivity which can be upgraded by nonlinear regression methods. The estimated inverted impedance surface of the C-sand interval using the model-based post-stack inversion procedure was converted to porosity in (Figure 6.10). High value impedance value in the C-sand interval follows a SW to NE direction, which is not a good distribution of porosity, according to the impedance surface. Porosity ranges between 0.03% to 0.04%. (Light blue color). The typical porosity is close to well Tajjal-01 and is around 0.03%. (Light red to dark cyan color).

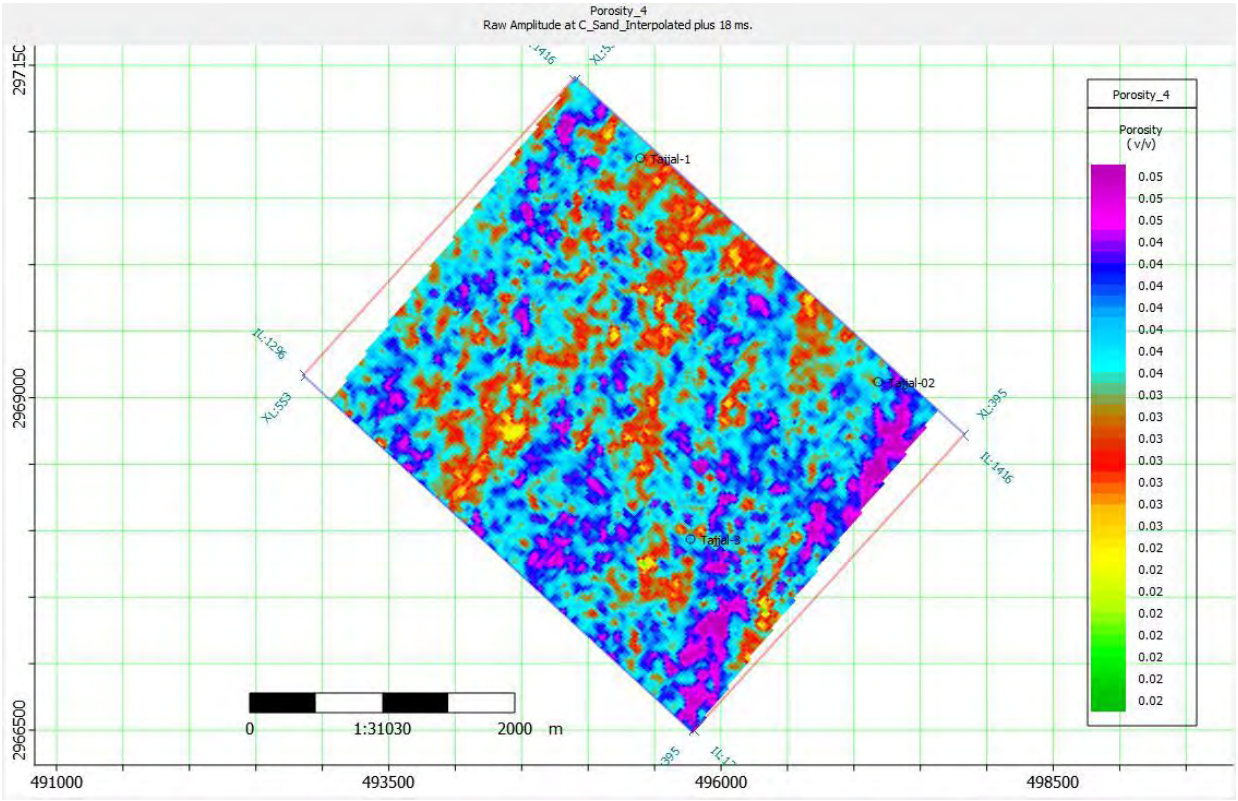

Figure 5.10: The distribution of porosity in the C-sand for the Gambat Latif block as determined by the findings of seismic inversion. A fraction is used to represent porosity.

CHAPTER 6
LAMBDA RHO AND MU RHO

6.1 Lambda Rho Section Tajjal-01 and Tajjal -02

Distinct facies can be easily differentiated using the Lambda-Mu-Rho (LMR) cross-plot method (Goodway et al. 1997; Das and Chatterjee 2018). The bulk impedance (incompressibility) and the shear impedance (rigidity), also known as Lambda-Rho and Mu-Rho, respectively, are particularly sensitive to the impact of fluid. Hydrocarbon sands show low Lambda-Rho incompressibility values (Goodway et al. 1997; Das and Chatterjee 2018). Results from applying the LMR cross-plot method on Tajjal-01 and Tajjal-02. Gas sand, tight sand, shaly gas sand, and shale facies are identified based on the cutoff values of Lambda- Rho and Mu-Rho (Goodway et al. 1997;). On the other hand, the incompressibility parameter Lambda-Rho is derived from P-waves. A rock's fluid type and saturation must alter in order to determine its composition. The incompressibility of a rock will gradually decrease significantly with a systematic switch from brine to oil to gas.

In the C interval Formation, a layer of sand with a high Lambda Rho value (35-45 Gpa * g/cc) is visible. It has been noted that the values of lambda RHo at Tajjal-01 and Tajjal-02 are more than (45 Gpa * g/cc). In (figures 6.1 and 6.2), density is low around Tajjal-01 compared to Tajjal-02. Low effective porosity may arise due to high density's potential to represent vast matrix volumes with fewer pores, yet billed with mineral or saline water rather than oil and gas.

Decreased Lambda value While high Rho levels are consistent with the lithology of shale, low Rho values indicate the presence of hydrocarbon-bearing sand. Rho indicates that sand is present. (Figures 6.1 and 6.2) show this. The property derived from the inversion has a substantial correlation with the well log, as shown by lambda-Rho cross sections. Both the reservoir interval and the B interval's high Lambda-rho values suggest the presence of hydrocarbon. On the zone that was exploited, there were two reservoirs.it was noted. This trend may be caused by the presence of the hydrocarbon gas carrying zone. Porosities of C sand were overlaid on the whole study area we concluded that lambda rho values are low at well positions indicates the presence of fluid (Figure6.3), the values are ranging from 26- 45 (Gpa * g/cc) with different color bar as shown in (Figure 6.3).

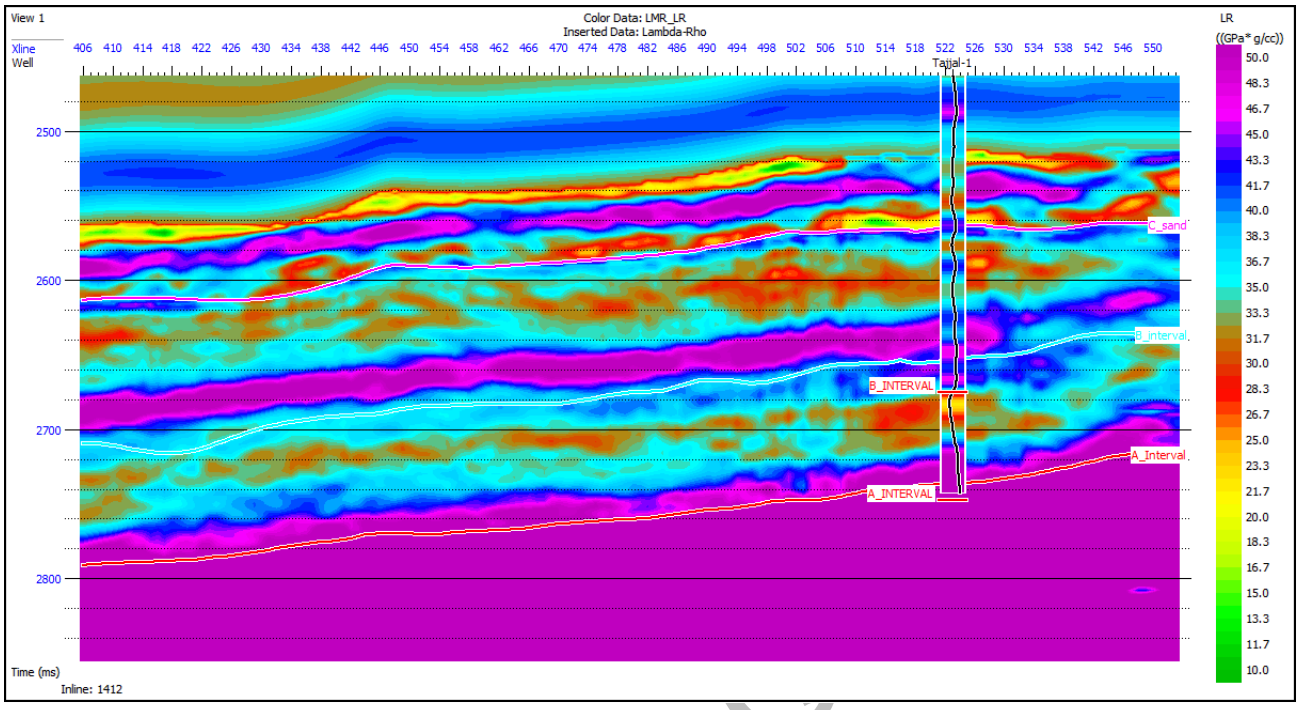

Figure 6.1: Representing the Lambda Rho of Tajjal 01

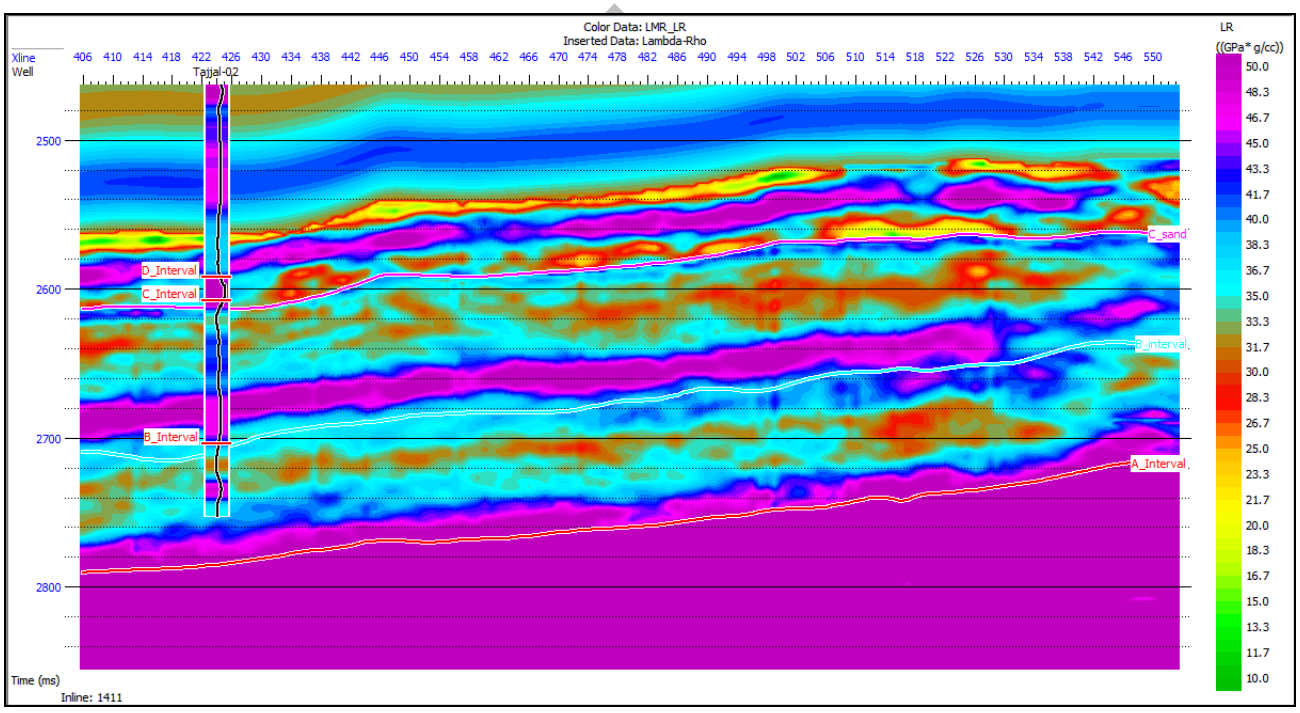

Figure 6.2: Representing the Lambda Rho of Tajjal -02.

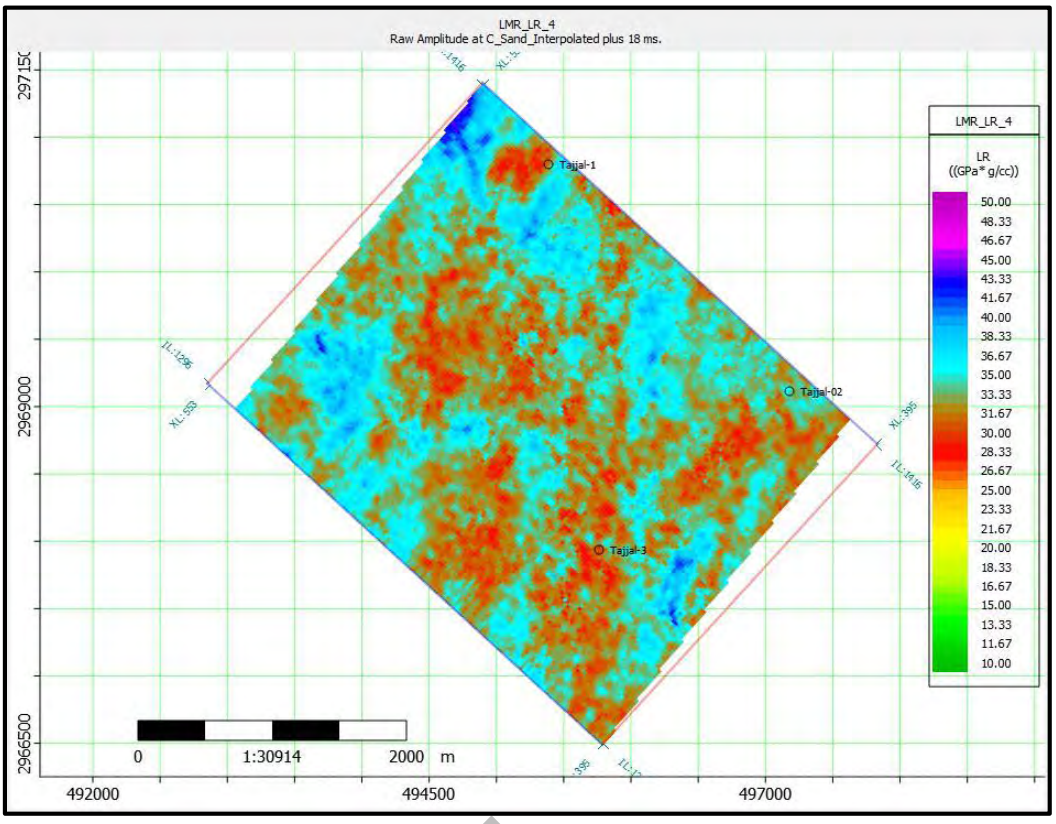

Figure 6.3: Representing the LMR LR slice at study area Mu Rho Section of Tajjal-01 and Tajjal -02

6.2 Mu Rho Section of Tajjal-01 and Tajjal -02

S-waves can be used to determine the amount Mu, or stiffness. It is anticipated that it will having a high value in sand than in shale because the sand matrix provides more resistance to shearing than the shale matrix will. Fluid in the pore spaces has no bearing on its value, it is envisaged that the value of brine and hydrocarbon fill sand will remain mostly unchanged. A suitable lithology indication for clastic is hence its product's bulk density, with high values indicating sand (Goodway et al. 1997). A decreased value for Mu-Rho, its product with the bulk density of the rock, is consistent with gas sand.

It has been shown that Mu-Rho is a reliable lithology indicator. The inversion result's cross section (Figure 6.4 and 6.5). The inversion result was quite good, as evidenced by the Mu-rho log's excellent correlation with the retrieved cross section superimposed on the cross section along Tajjal-01 and Tajjal-02. According to the tale and the findings of our thorough investigation, sand is present when Mu-Rho has a very high value. High Mu-Rho values in the explored zone correspond to intervals with low gamma ray values when sand is found at B and C intervals. A high Mu-Rho value was also discovered in the prospective region, pointing to the

presence of good sands with gas-bearing zones in Tajjal-01 and Tajjal-02. Mu Rho values range from 51 to 54 (Gpa * g/cc) in the C interval at Tajjal-01, and from 47 to 50 (Gpa * g/cc) at Tajjal-02 (Figure 6.4 and 6.5). As values of MU RHO are overlaid on the complete study area or well location through there, we can see the response of MU RHO that is relatively high 25 to 45 (Gpa * g/cc) represented by color bar indicating presence of tight sands on the well locations of Tajjal-01 and Tajjal-02. As impedance slice is also made in order to get a broad view of the density and velocity at the well location of Tajjal-01 and Tajjal-02 at Tajjal -01 values are high showing density and velocity is very high so tight sands while at Tajjal-02 showing a relatively low values of impedance displayed by the color bar showing a relatively loose sands present at Tajjal-02 as (Figure 6.5). In Figure 6.7 slice was also made of MU rho representing the values along the color bar.

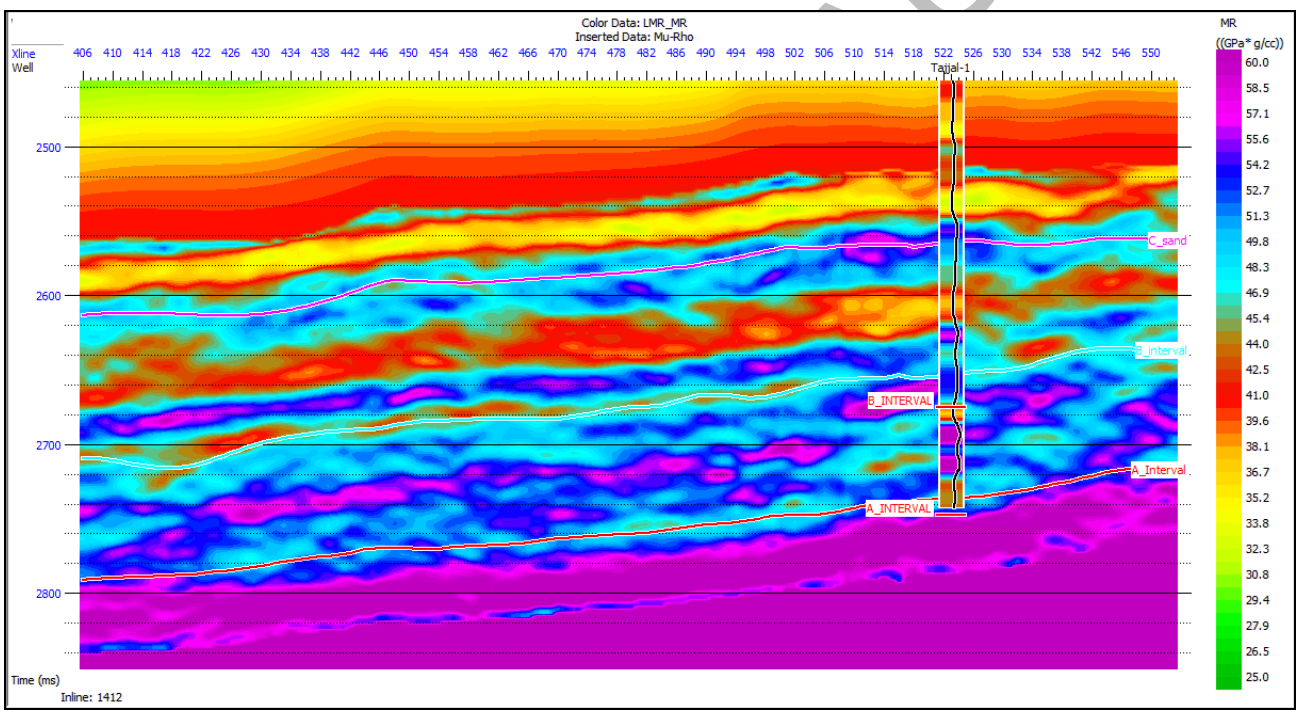

Figure 6.4: Mu Rho Section of Tajjal-01.

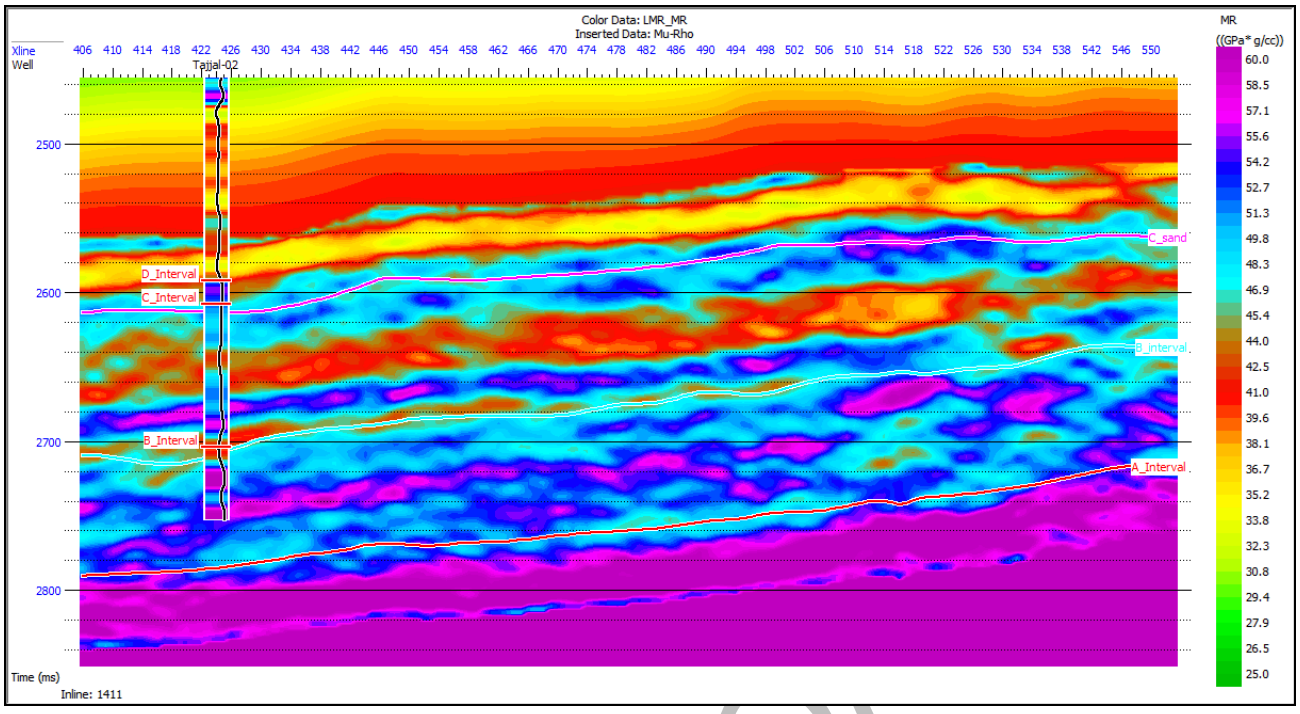

Figure 6.5: Mu Rho Section of Tajjal-02

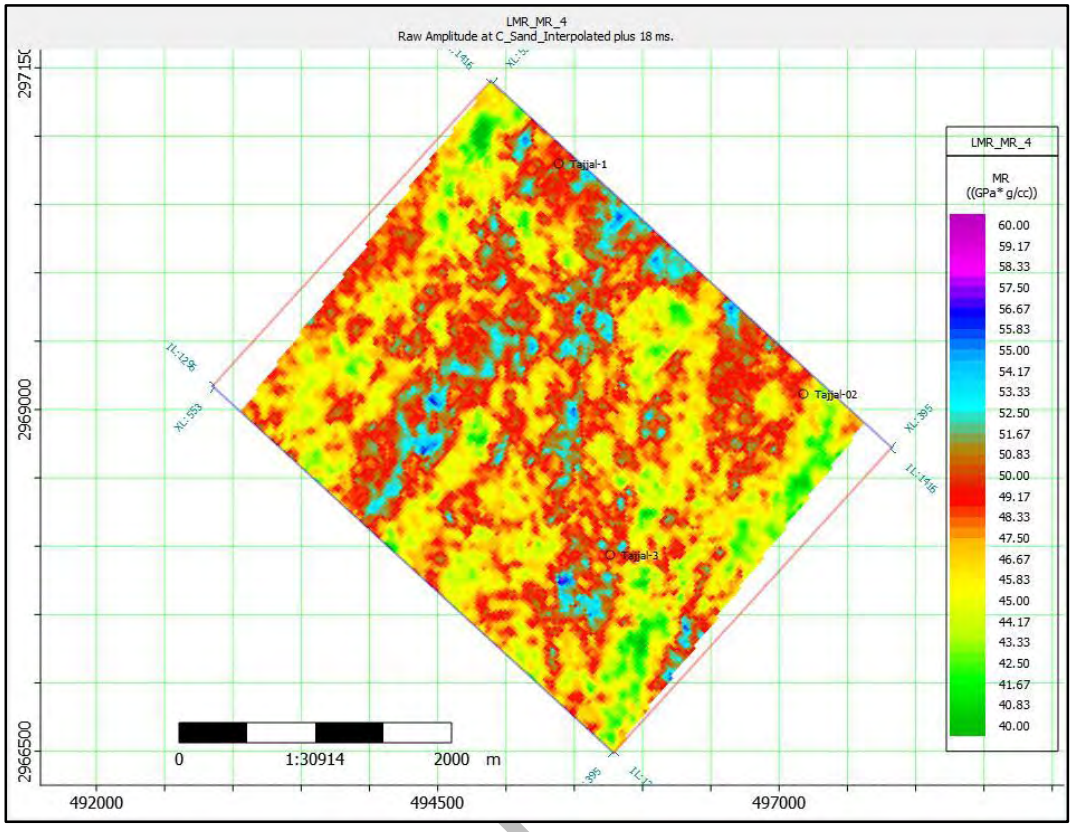

Figure 6.6: Representing the MU Rho slice on the study area Gambat Latif.

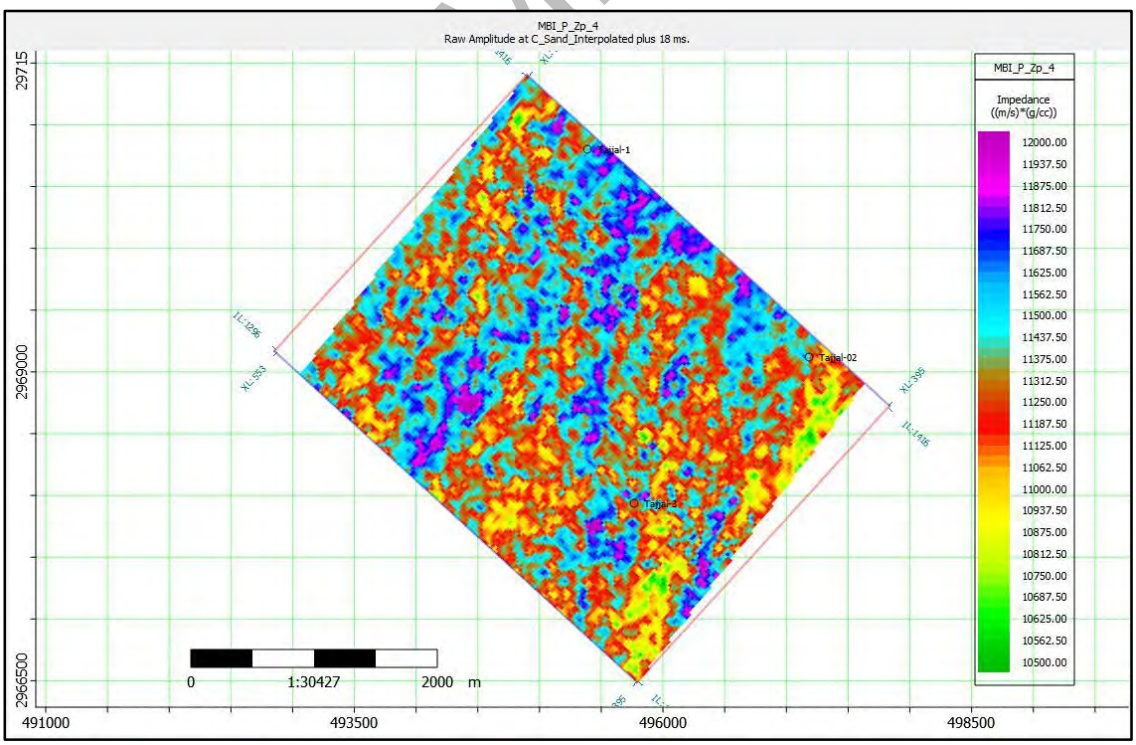

Figure 6.7: Representing the impedance slice of the study area

The cross plot between the lambda rho on the x axis and the mu rho on the y axis, coupled with the color bar of the P impedance values, is in (Figure 6.8). The dispersion of the points with different colors are showing which area is having brine water, gas, oil and shale etc. At those points where the value of lambda rho is less and Mu rho is high showing the gas zone classified as gas sands. As in previous chapter 6 P impedance is shown the values of p impedance is relatively low at C sand showing the presence of gas sands at that area which is justified by this plot along with Lambda Rho and MU rho sections are also showing the values contrast at that particular well Tajjal -01. Petro physical interpretation of well Tajjal - 01 is also justifying the results of the cross plots made in this chapter in order to determine their porosities. Additionally, we used the Lambda-Mu-Rho cross-plot method to effectively distinguish between various facies (Goodway et al. 1997; Das and Chatterjee 2018). In particular, Lambda-Rho and Mu-Rho are extremely sensitive to the impact of fluid because they represent the bulk impedance (incompressibility) and the shear impedance (rigidity), respectively. Low incompressibility values for Lambda-Rho are observed in hydrocarbon sands (Goodway et al. 1997; Das and Chatterjee 2018). The outcome of the LMR cross-validation in (Figure 6.8).

On the basis of cut-off values of Lambda-Rho and Mu-Rho, gas sand, tight sand, shaly gas sand, and shale facies are recognized by evaluating the values of Tajjal-01 (Goodway et al.1999).

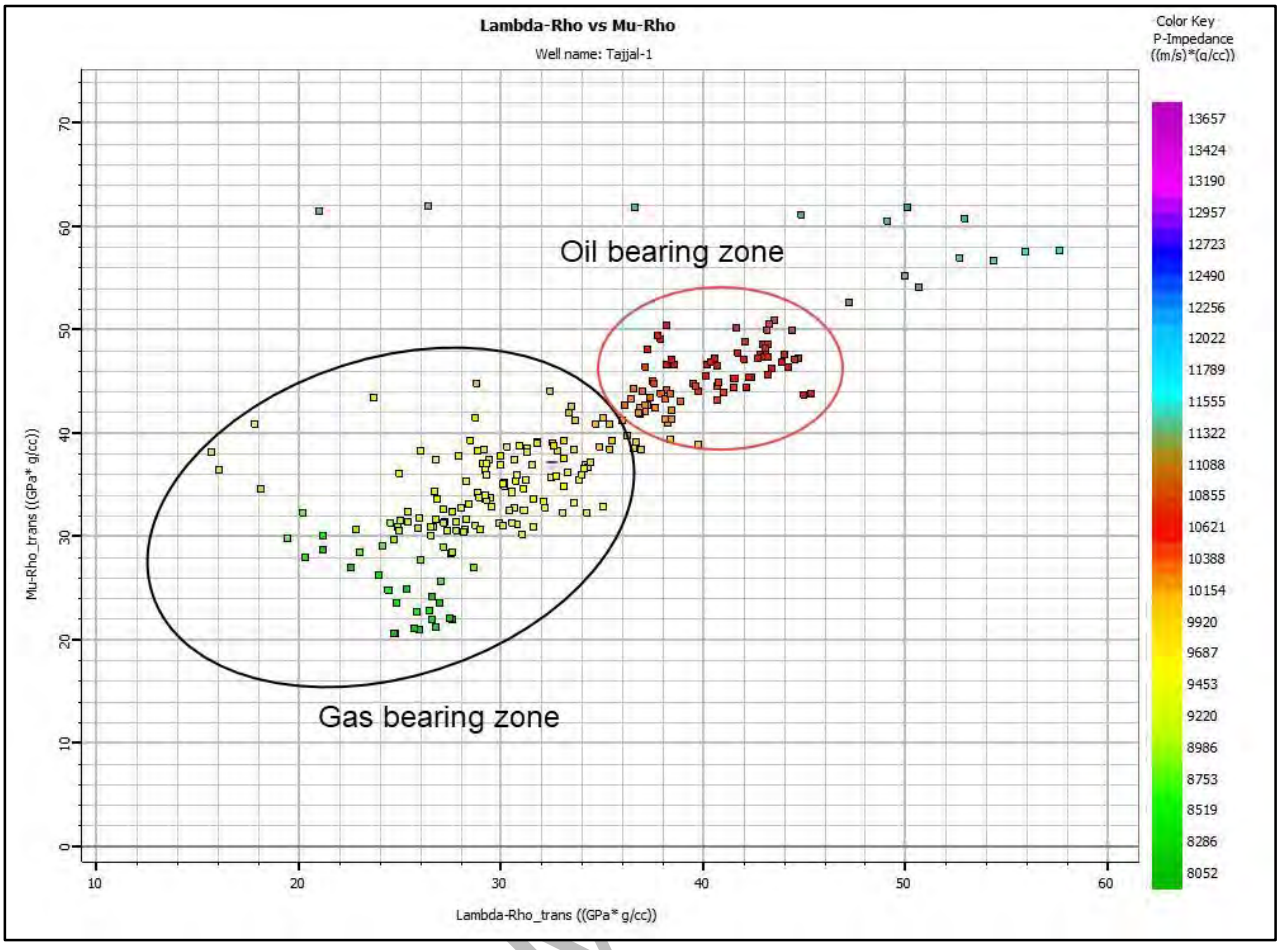

Figure 6.8: Representing the cross plot of lambda Rho and MU Rho vs P impedance

6.3 Reservoir character (porosity) estimation

Figure 6.9 shows the cross plot of P impedance and Effective porosity. There has been discovered a good correlation coefficient. Linear regression method was helpful in the correlation coefficient. One can forcefully fit the data using a higher order polynomial, splines, and other mathematical techniques. Since the link between estimated porosity and acoustic impedance is linear in nature, we used a linear regression technique. As a result, with a correlation of 79%, the porosity prediction using inverted acoustic impedance is reasonable given this particular geological scenario. Since impedance decreases as porosity values increase, there is a linear relationship between P impedance and effective porosity with a negative slope. Cross plot between acoustic impedance and porosity has been made at the well location Tajjal-01, shown in (Figure 6.9), using their average values. At the well location Tajjal-01, the average values of acoustic impedance and porosity were used to create a cross plot (Figure6.9).

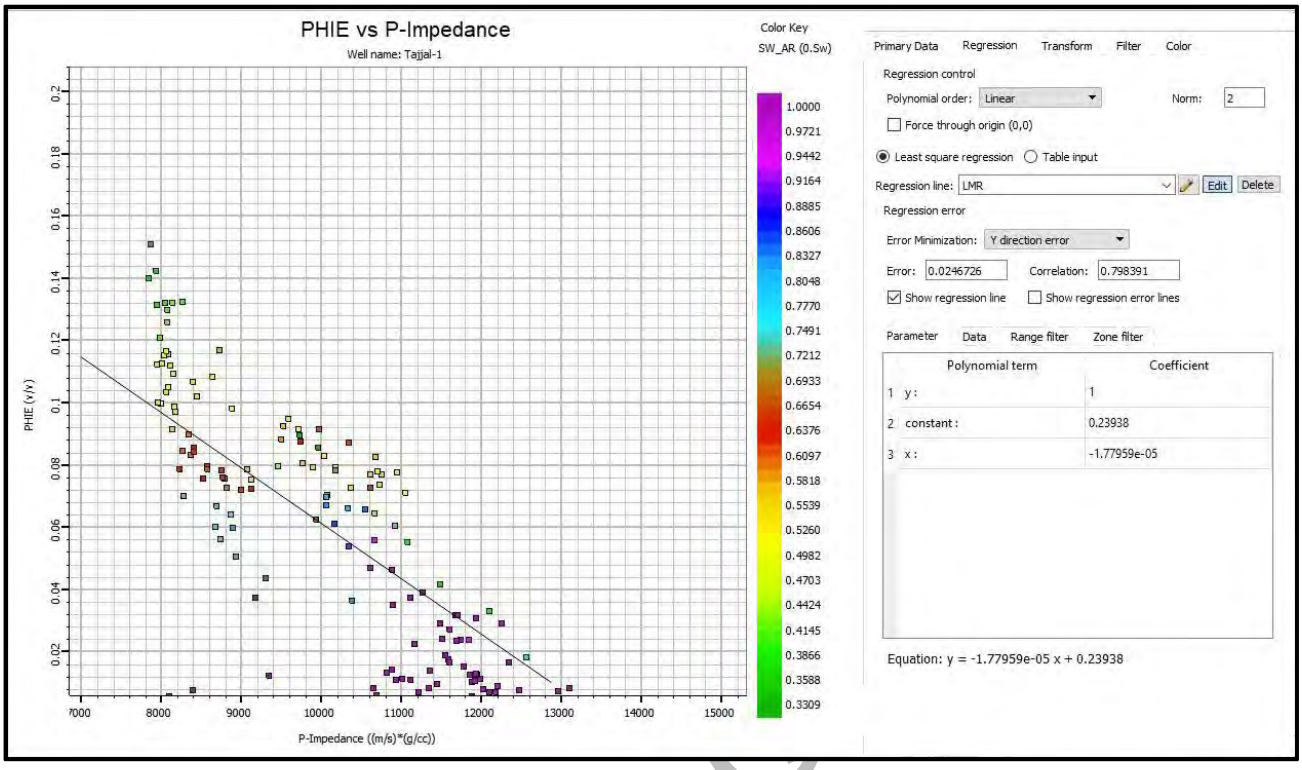

Figure 6.9: Cross plot of P impedance and Effective porosity with a respectable correlation coefficient value Effective porosity and P impedance have a constant linear relationship with a negative slope.

DISCUSSION AND CONCLUSIONS

Three reflectors named as Lower Goru Formation, C interval, and B Interval have been identified and marked at specific times after confirmation form synthetic seismogram generated from well log data of Tajjal-01. Results from geophysical examination confirms the presence of normal faul under extensional regime in the study area which can be clearly visualized on the seismic sections. Reservoirs from multiple petroleum plays have been observed within Gambat Block that is B interval of Lower cretaceous age. Furthermore, time and depth contour maps confirm the lateral extension of faults in NW-SE direction in the Lower Goru and the lateral fault polygon orientation in the Lower Goru show N-S orientation. The fault polygons on the contour maps depict the plane of discontinuity that give us a pictorial display of subsurface horst and graben structures.

Calculations of Petro physical attributes contributes in confirmation of hydrocarbon bearing strata. In this research work, reservoir properties of one well i.e., Tajjal 01 was calculated through petrophysical interpretation. According to Khan et al., (2016), B interval is an excellent gas reservoir possessing vuggy and inter-crystalline porosity consequently C interval in given data set, depicts good reservoir qualities and volume of 39.4%, and effective porosity of 12.6%, and water saturation of 12.6 % and hydrocarbon saturation is 87.4% for zone 1 and for Zone 2 42% volume of shale. The effective porosity of C interval is greater than 12.1%. Water saturation ranges from 19.5%, while hydrocarbon saturation ranges from 80.5%.

Post-stack seismic inversion gives layer property in the form of acoustic impedance. This property can be used to determine presence of hydrocarbons as it is a product of velocity and density. The results of inversion can either be relative or absolute depending upon the methodology being used. In case of Model Based inversion the results are in the form of relative values. Model based inversion performed on inline 1412 gives low acoustic impedance within C interval and B interval thus providing further evidence of presence of hydrocarbons.

Porosity is a valuable property which is obtainable from seismic data with the help of different control points (well location) after inversion analysis. Due to the fact that porosity and impedance

are inversely linked, a linear relation is formulated between effective porosity values and inverted impedance. This relation has been applied to seismic inline 1412 with Tajjal-01 being used as control point to observe lateral variations of porosity distribution on the seismic section. The porosity distribution observed on the section holds consistency with the well based porosity values. Both B and C interval has v=better results for model-based inversion because it has shallow depth and hence high frequency waves can travel up-to and from this formation without any dispersion. Which results in better resolution and hence better results. But it may have relatively lesser porosity distribution in C and B interval

Following are the conclusions of this study:

1. According to the area's seismic interpretation, there are horst and graben structures that are surrounded by normal faults that were created during an extensional era.
2. Time and Depth contour maps confirm the shape of sub-surface structures (horst and graben) within the region as well as the lateral extension and orientation of the fault polygons.
3. Petro physical analysis on Tajjal 01 was performed using well log data. Petro physical interpretation of Tajjal_01 confirms that well Tajjal-01 shows presence of hydrocarbons. Tajjal_01 has 39.4% volume of shale. The effective porosity of C interval is greater than 12.6%. Water saturation ranges from 12.6%, while hydrocarbon saturation ranges from 87.4% in zone 1. Zone 2 has 42% volume of shale. The effective porosity of C interval is greater than 12.1%. Water saturation ranges from 19.5%, while hydrocarbon saturation ranges from 80.5% in zone 2.
4. Model Based inversion performed on the inline 1412 further demonstrates an evident presence of hydrocarbon potential within B interval and C interval respectively. Porosity estimation from post stack seismic colored inversion gives Moderate values for B interval and C interval in Tajjal-01 thus indicating the presence of hydrocarbon potential
5. The identification and delineation of hydrocarbon-charged sands with increased confidence were made possible by the combined interpretation of $\lambda\rho$ and $\mu\rho$ from the post-stack 3D seismic data set in the research area the presence of gas along the zone of interest is confirmed by the low $\lambda\rho$ values with the moderate values of $\mu\rho$ depicting the presence of sand lithology.

REFERENCES

Aamir, A., Matee, U., Matloob, H., Bhatti, A. S., & Khaista, R. (2017). Estimation of the shale oil/gas potential of a Paleocene–Eocene succession: A case study from the Meyal area, Potwar Basin, Pakistan.

Acta Geologica Sinica-English Edition, 91(6), 2180-2199.Al-Rahim, A. M., & Hashem, H. A. (2016). Subsurface 3D prediction porosity model from converted seismic and well data using model-based inversion technique. Iraqi Journal of Science, 57(1A), 163-174.

Archie, G. E. (1950). Introduction to petrophysics of reservoir rocks. AAPG bulletin, 34(5), 943-961.

Asquith, G. B. and Gibson, C. R. (1982). Basic well log analysis for geologists. American Association of Petroleum Geologists, Tulsa,216.

Asquith, G. B., Krygowski, D., & Gibson, C. R. (2004). Basic well log analysis (Vol. 16). Tulsa: American association of petroleum geologists.

Azeem, I., Walterscheid, R. L., Crowley, G., Bishop, R. L., & Christensen, A. B. (2016). Observations of the migrating semidiurnal and quaddiurnal tides from the RAIDS/NIRS instrument. Journal of Geophysical Research: Space Physics, 121(5), 4626-4637.

Bacon, C. R., Sisson, T. W., & Mazdab, F. K. (2007). Young cumulate complex beneath Veniaminof caldera, Aleutian arc, dated by zircon in erupted plutonic blocks. Geology, 35(6), 491-494.

Badley, M. E. (1985). Practical seismic interpretation.

Bakker, P. (2002). Image structure analysis for seismic interpretation (pp. 32-34).

Bannert, D., Cheema, A., Ahmed, A., & Schäffer, U. (1993). The Structural Development of the Western Fold Belt, -Pakistan.

Barclay, F., Bruun, A., Rasmussen, K. B., Alfaro, J. C., Cooke, A., Cooke, D., & Roberts, R. (2008). Seismic inversion: Reading between the lines. Oilfield Review, 20(1), 42-63.53

Bjorlykke, K. (2010). Petroleum geoscience: From sedimentary environments to rock physics. Springer Science & Business Media.

Bjørlykke, K., Jahren, J., 2010. Sandstones and sandstone reservoirs. In: Bjørlykke, K. (Ed.), Petroleum Geoscience. Springer-Verlag, From Sedimentary Environments to Rock Physics, pp. 113–140.

Bone, M. R., Giles, B. F., & Tegland, E. R. (1977). Geologic Interpretation of 3-D Seismic Data.

Bosch M, Carvajal C, Rodrigues J, Torres A, Aldana M and Sierra J 2009 Petrophysical seismic inversion conditioned towell-log data: Methods and application to a gas reservoir; Geophysics 74 O1–O15, https://doi.org/10.1190/1.3043796.

Bosch M, Mukerji T and Gonzalez E F 2010 Seismic inversion for reservoir properties combining statistical rock physics and geostatistics: A review; Geophysics 75 75A165, https://doi.org/10.1190/1.3478209.

Caers J, Avseth P and Mukerji T 2001 Geostatistical integration of rock physics, seismic amplitudes, and geologic models in North Sea turbidite systems; Lead Edge 20308, https://doi.org/10.1190/1.1438936.

Chen Q and Sidney S 1997 Seismic attribute technology for reservoir forecasting and monitoring; Lead Edge 16445–448, https://doi.org/10.1190/1.1437657.

Chopra S and Marfurt K J 2007 Seismic attributes for prospect identification and reservoir characterization; Geophys. Dev.Ser. 11 465, https://doi.org/10.1190/1.9781560801900.

Das B and Chatterjee R 2016 Porosity mapping from inversion of post–stack seismic data; Georesursy 18(4) 306–313.

Das B and Chatterjee R 2018 Well log data analysis for lithology and fluid identification in Krishna–GodavariBasin, India; Arab. J. Geosci. 11(10) 231.

Chopra, S., & Marfurt, K. J. (2005). Seismic attributes—A historical perspective. Geophysics, 70(5), 3SO-28SO.

Coffeen, J.A., 1986, Seismic Exploration Fundamentals, PennWell Publishing Co,

Cooke, D., & Can't, J. (2010). Model-based Seismic Inversion: Comparing deterministic and probabilistic approaches. CSEG Recorder, 28-39

Cooper, G. (2004). The stable downward continuation of potential field data. Exploration Geophysics, 35(4), 260-265.

Cosgrove, J. W. (1998). The role of structural geology in reservoir characterization. Geological Society, London, Special Publications, 127(1), 1-13.

Castagna, J.P., Batzle, M.L., and Kan, T.K., 1993. Rock physics – The link between rock properties and AVO response. In Offset-Dependent Reflectivity – Theory and Practice of AVO

Analysis, ed. J.P. Castagna and M. Backus. Investigations in Geophysics, No. 8, Society of Exploration Geophysicists, Tulsa, Oklahoma, pp. 135–171.

Daniel, P., & McPherson, C. (2004, March). Overview of the Issues. In Petroleum Revenue Management Workshop (p. 5).

Dobrin, M. B., and C. H. Savit. "Introduction to Geophysical Prospecting McGraw-Hill Book Co." New York (867 pp.) (1988).

Da-Xing, W. A. N. G. (2017). A study on the rock physics model of gas reservoir in tight sandstone. Chinese Journal of Geophysics, 60(1), 64-83.

Eames, F.E. 1952. A contribution to the study of the Eocene in western Pakistan and western India; Part A. The geology of standard sections Lower Cenozoic of Pakistan Greater Indus Basin 21 in the western Punjab and in the Kohat District. Quarterly Journal of the Geological Society of London, 107: 159–171.54

Fajana, A. O. (2021). Analytical modeling of effect of volume of shale different calculation methods on reservoir petrophysical parameters. Earth Science Informatics, 14(1), 543-561.

Fatmi, A. N., & AN, F. (1977). Neocomian ammonites from northern areas of Pakistan.

Gadallah, Mamdouh R., and Ray Fisher. "Seismic Interpretation." Exploration Geophysics. Springer, Berlin, Heidelberg, 2009. 149-221

Gavotti, P. E. (2014). Model-based inversion of broadband seismic data.

Gavotti, P., Lawton, D., Margrave, G., & Isaac, H. (2013). Post stack inversion of broadband seismic data from Alberta, Canada. In SEG Technical Program Expanded Abstracts 2013 (pp. 3149-3153). Society of Exploration Geophysicists.

Gibson, G. M. (1982). Stratigraphy and petrography of some metasediments and associated intrusive rocks from central Fiordland, New Zealand. New Zealand journal of geology and geophysics, 25(1), 21-43.

Handwerger, B. (2004). Predictors of neuropsychiatric damage in systemic lupus.

HEMPHILL, W. R. • KIDWA1, A. H. 1973. Stratigraphy of the Bannu and Dera lsmail Khan areas, Pakistan. United States Geological Survey Professional Paper, 716-B.

Hinsch, R., Hagedorn, P., Asmar, C., Nasim, M., Aamir Rasheed, M., & Kiely, J. M. (2017, April). Deformation and kinematics of the central Kirthar Fold Belt, Pakistan. In EGU General Assembly Conference Abstracts (p. 12284).

Jain, C. (2013). Effect of seismic wavelet phase on post stack inversion. In 10th Biennial Int. Conf. & Exposition, Kochi (p. 410).

Kadri, I. B. (1995). Petroleum geology of Pakistan. Pakistan Petroleum Limited.

KAZMI, A. H. & JA N, M. Q. 1997. Geology and Tectonics of Pakistan.

Kerzner, M., & Daniel, P. J. (2018). Big Data in Oil & Gas and

Petrophysics. In Guide to Big Data Applications (pp. 175-204). Springer, Cham.

Kneller, E. A., Albertz, M., Karner, G. D., & Johnson, C. A. (2013). Testing inverse kinematic models of paleo crustal thickness in extensional systems with high-resolution forward thermo-mechanical models. Geochemistry, Geophysics, Geosystems, 14(7), 2383-2398.55

Latif, M. A. 1964. Variations in abundance and morphology of pelagic Foraminifera in the Paleocene-Eocene of the Rakhi Nala, West Pakistan. Geological Bulletin of Punjab University, Lahore 4:29-100.

Lindseth, R. O. (1979). Synthetic sonic logs—A process for stratigraphic interpretation. Geophysics, 44(1), 3-26.

G. Mavko, T. Mukerji, J. DvorkinThe Rock Physics Handbook: Tools for SEISMIC analysis of Porous MediaCambridge University Press (2009),

Meissner JrC, Rahman H (1973) Distribution, thickness, and Lithology of Paleocene Rocks in Pakistan. In: USGS Professional Paper 716-E, US Government Office, Washington.

Niamatullah, M., & Imran, M. (2012). Structural geometry and tectonics of southern part of Karachi arc—a case study of Pirmangho and Lalji area. Search and Discovery Article, 50581.

Oldenburg, D. W., T. Scheuer, and S. Levy. "Recovery of the acoustic impedance from reflection seismograms." Geophysics 48.10 (1983): 1318-1337.

Patella, D. (1974). On the transformation of dipole to Schlumberger sounding curves. Geophysical Prospecting, 22(2), 315-329.

Shakir, U., Ali, A., Amjad, M. R., & Hussain, M. (2021). Improved gas sand facies classification and enhanced reservoir description based on calibrated rock physics modelling: A case study. Open Geosciences, 13(1), 1476-1493.

Sen, M. K. (2006). Seismic inversion. Richardson, TX.: Society of Petroleum Engineers.

Shah, T. (2009). Climate change and groundwater: India’s opportunities for mitigation and adaptation. Environmental Research Letters, 4(3), 035005.

Sheriff, R. E, 1999, Encyclopedic dictionary of exploration Geophysics (Third Edition): Soc. Expl. Geophysics., 180.

Simm, R., Bacon, M., & Bacon, M. (2014). Seismic Amplitude: An interpreter's handbook. Cambridge University Press.

Smewing, J. D., Warburton, J., Daley, T., Copestake. P., and Ul-Haq, N.: Sequence stratigraphy of the southern Kirthar Fold Belt and Middle Indus Basin, Pakistan, in: The Tectonic and 56
Climatic Evolution of the Arabian Sea Region, edited by: Clift, P. D., Kroon, D., Gaedicke, C., and Craik, J., Geol. Soc. Spec. Publ., 195, 273–299, 2002b

Sroor, M. (2010). Geology and geophysics in oil exploration. Mahmoud Ahmed Sroor.

Telford, W. M., Geldart, L. P., and Sheriff, R. F., 1990, Applied Geophysics, 2nd Ed., Cambridge Univ. Press. Thompson, D. T., 1982, EULDPH: A new technique for making computer-assisted depth estimates from magnetic data: Geophysics, 47, 31–37.

Tittman, J., & Wahl, J. S. (1965). The physical foundations of formation density logging (gamma-gamma). Geophysics, 30(2), 284-294.

Yilmaz, Ö. (2001). Seismic data analysis: Processing, inversion, and interpretation of seismic data. Society of exploration geophysicists.

Zaigham, N. A., & Mallick, K. A. (2000). Prospect of hydrocarbon associated with fossil-rift structures of the southern Indus basin, Pakistan. AAPG bulletin, 84(11), 1833-1848.

Zemke, K., Liebscher, A., & Wandrey, M. (2010). Petrophysical analysis to investigate the effects of carbon dioxide storage in a subsurface saline aquifer at Ketzin, Germany (CO2SINK). International Journal of Greenhouse Gas Control, 4(6), 990-999.